Chemical Geology 328 (2012) 259–277

Contents lists available at SciVerse ScienceDirect

Chemical Geology

journal homepage: www.elsevier.com/locate/chemgeo

Tholeiite–Boninite terrane in the North Qilian suture zone: Implications for subduction initiation and back-arc basin development

Xiaohong Xia [a], Shuguang Song [a,*], Yaoling Niu [b,c]

[a] MOE Key Laboratory of Orogenic Belts and Crustal Evolution, School of Earth and Space Sciences, Peking University, Beijing 100871, China
[b] School of Earth Sciences, Lanzhou University, Lanzhou 730000, China
[c] Department of Earth Sciences, Durham University, Durham DH1 3LE, UK

ARTICLE INFO

Article history:
Accepted 1 December 2011
Available online 8 December 2011

Keywords:
Tholeiite
High-Ca boninite
Infant arc magmatism
Back-arc basin
North Qilian suture zone

ABSTRACT

A tholeiite–boninite terrane occurs as a ~4.5-km-thick massif with lavas and intrusions in the Dachadaban (DCDB) area, the middle part of the North Qilian oceanic-type suture zone. It comprises two distinct lithological groups: the lower tholeiite unit and the upper boninite unit. The lower tholeiite unit consists of massive lava flows and subordinate gabbro intrusions with MORB-like characteristics that could represent 5–6% melting of an enriched MORB mantle. In contrast, the overlying boninite unit consists of pillow lavas, dolerite dykes and gabbro intrusions and shows high-Ca boninite features that may be formed by continuous melting of the extremely refractory mantle with the aid of a combination of the elevated mantle potential temperature of 1380–1460 °C at depths of 42–66 km and involvement of slab-derived hydrous fluids/melts. Zircon U–Pb SHRIMP dating shows that lower tholeiite magmatism lasted for at least 12 M.y. from 517 Ma to 505 Ma and upper boninite volcanism occurred between 505 and 487 Ma, which is consistent with the earliest age (486 ± 7 Ma) of the SSZ-type ophiolite belt immediately north of the Dachaidaban (DCDB) tholeiite–boninite terrane. The lower tholeiites are considered to represent the products of earliest infant arc magmatism by decompression-induced partial melting of the relatively "dry" and fertile upwelling mantle in response to the onset of subduction. The upper boninite unit with younger age of 487 ± 9 Ma is interpreted as earliest products of infant arc splitting and subsequent back-arc basin development. Therefore, the long-lived DCDB tholeiite–boninite sequence presents a key lithological record of early stages of supra-subduction zone magmatic activity evolved from subduction initiation at ~517 Ma to back-arc extension at ~487 Ma.

1. Introduction

A boninite is a relatively rare, but important primitive magma that currently erupts at modern arc—back-arc systems (e.g., Hawkins, 1976; Meijer, 1980; Crawford et al., 1981; Hickey and Frey, 1982; Reagan and Meijer, 1984; Falloon et al., 1987; Crawford et al., 1989; Boespflug et al., 1990; Pearce et al., 1992; Monzier et al., 1993; Hawkins and Castillo, 1998; Falloon et al., 2008; Niedermeier et al., 2008; Rubin et al., 2009). It has also been identified in a number of ophiolites and ophiolite-like terranes such as the Troodos ophiolite (e.g., Cameron, 1985; Flower and Levine, 1987), the Koh ophiolite (Sameshima et al., 1983; Meffre et al., 1996) and the Betts Cove ophiolite (Bédard et al., 1998; Bédard, 1999). Experimental studies and trace element modeling have shown that, in addition to the effect of water, elevated mantle potential temperature and mantle decompression are required to produce boninite magmas (Mysen and Kushiro, 1977; Flower and Levine, 1987; Sobolev and Danyushevsky, 1994; Bédard, 1999; Falloon and Danyushevsky, 2000; Sugawara, 2000). Boninites and boninite-like terranes are thus considered to be products of lithospheric extension and asthenospheric upwelling in response to the initiation of a subduction zone or back-arc opening (Crawford et al., 1981; Hickey and Frey, 1982; Tatsumi et al., 1983; Hawkins et al., 1984; Flower and Levine, 1987; Crawford et al., 1989; Falloon et al., 1992; Stern and Bloomer, 1992; Monzier et al., 1993; Meffre et al., 1996; Bédard et al., 1998; Bédard, 1999; Macpherson and Hall, 2001; Ishikawa et al., 2002; Hall et al., 2003; Ishizuka et al., 2006; Dilek and Thy, 2009; Pearce and Robinson, 2010).

Systematic stratigraphy, geochemistry and geochronology studies of boninite terranes from Izu-Bonin-Mariana (IBM) subduction system (Meijer, 1980; Arculus et al., 1992; Ishizuka et al., 2006; Dilek and Thy, 2009) have confirmed the view that boninites are generated through processes associated with subduction initiation and fore-arc extension (e.g., Stern and Bloomer, 1992; Bloomer et al., 1995; Hall et al., 2003; Stern, 2004). The subduction initiation model account for most geological and geophysical characteristics of the western Pacific Eocene boninite (Hall et al., 2003; Ishizuka et al., 2006) and has also been applied to the Central Asian SSZ ophiolite belt over thousands of kilometers (Dilek and Thy, 2009; Pearce and Robinson, 2010), the

* Corresponding author. Tel.: +86 10 62767729.
E-mail address: sgsong@pku.edu.cn (S. Song).

0009-2541/$ – see front matter © 2011 Elsevier B.V. All rights reserved.
doi:10.1016/j.chemgeo.2011.12.001

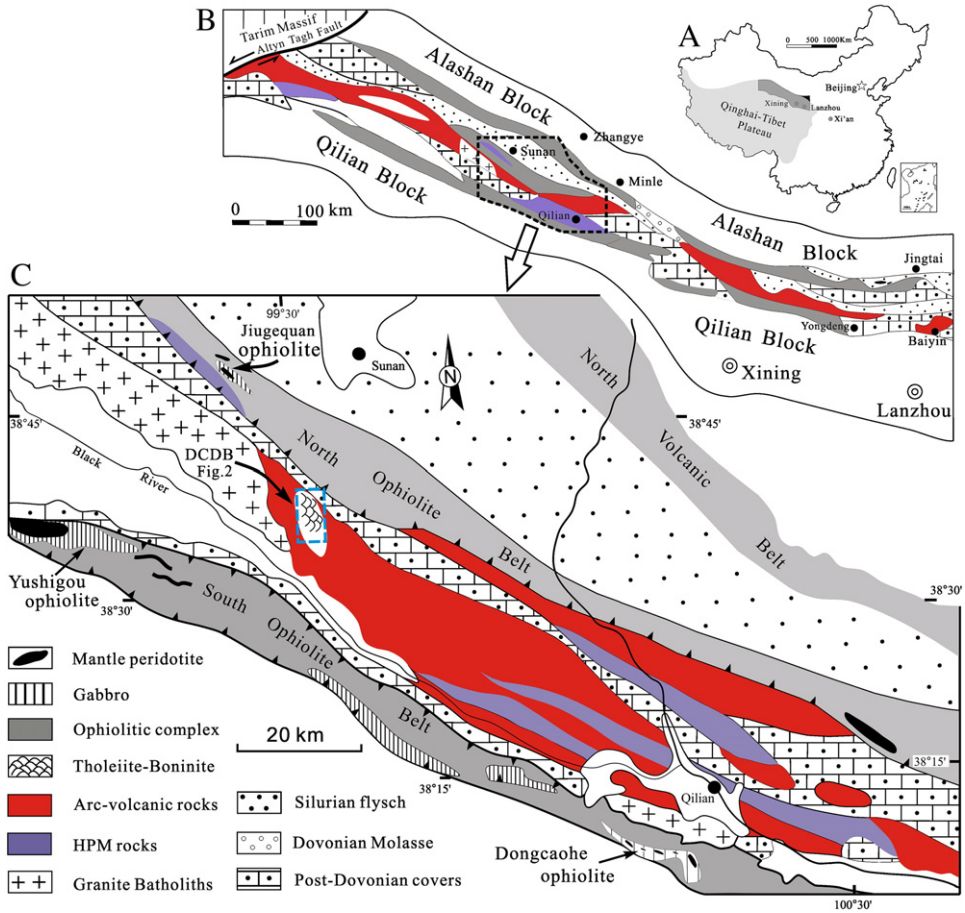

Fig. 1. (A) Schematic location for the North Qilian orogenic belt in Qinghai-Tibet plateau. (B) Geological map of the North Qilian Orogenic belt (simplified after Feng and He, 1995). (C) Enlarged area showing the locations of Dachadaban (DCDB) tholeiite–boninite terrane.
Modified after Song et al. (2007).

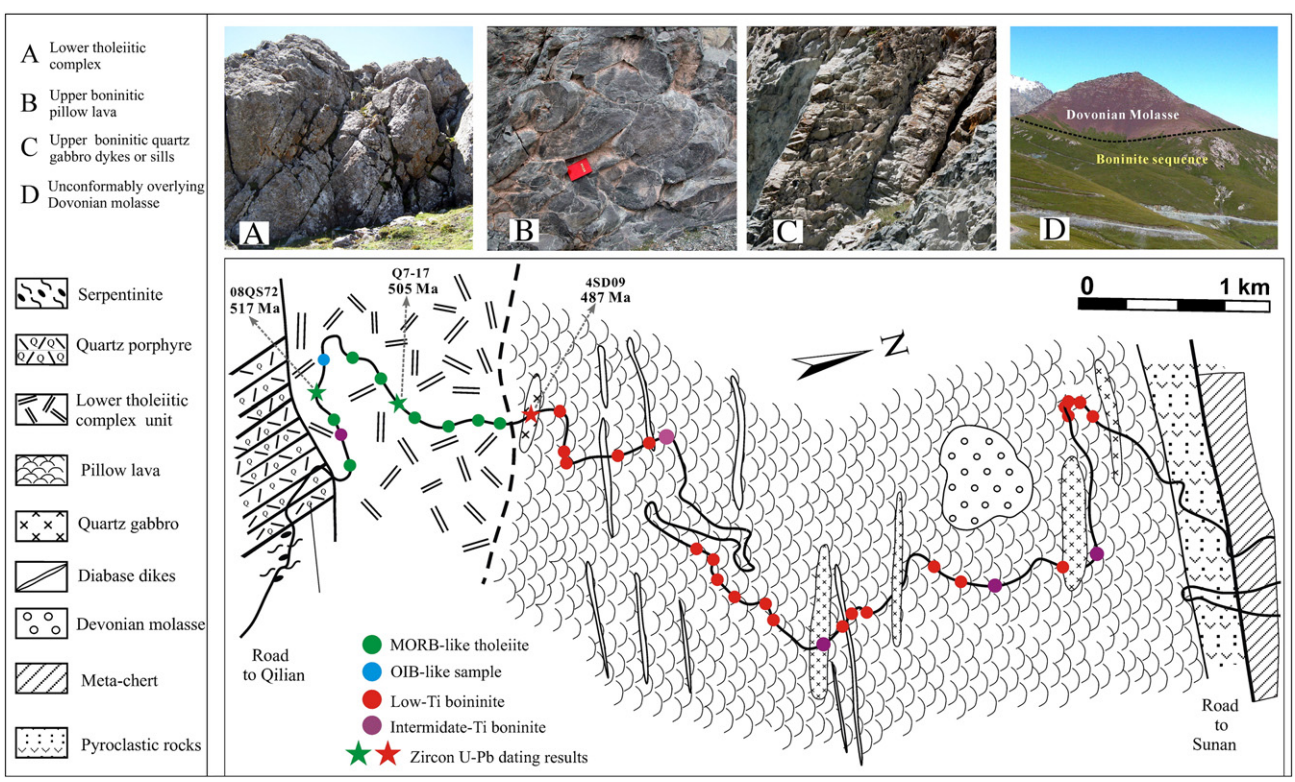

Fig. 2. Detailed geological map with field photos showing main lithological–geochemical units, stratigraphical relationships and sample types through DCDB tholeiite–boninite terrane.

Wild Bight Group and the South Lake Igneous Complex (MacLachlan and Dunning, 1998), the Betts Cove ophiolite (Bédard et al., 1998; Bédard, 1999), and the Thetford Mines ophiolite complex (Pagé et al., 2009). However, a number of boninites such as the Koh ophiolite (Sameshima et al., 1983; Meffre et al., 1996), the Oman ophiolite (Ishikawa et al., 2002) and the Troodos massif (e.g., Cameron, 1985; Flower and Levine, 1987) display significant differences from the fore-arc extension-related boninites in the geochemistry, mineralogy and rock association, but show a striking similarity to present-day occurrences in back-arc basins, such as the Lau basin (e.g., Hawkins, 1976; Boespflug et al., 1990; Falloon et al., 1992), North Tonga (e.g., Sobolev and Danyushevsky, 1994; Danyushevsky et al., 1995; Falloon et al., 2007), Hunter Ridge (Monzier et al., 1993; Sigurdsson et al., 2003) and Eastern Manus (Niedermeier et al., 2008; Rubin et al., 2009). The main differences between the two types of boninites include: (1) the fore-arc extension-related boninites are commonly associated with IAT or island arc andesite-dacite-rhyolite (ADR) series (Hickey and Frey, 1981, 1982; Bloomer and Hawkins, 1987; Murton et al., 1992; Taylor et al., 1994), whereas the back-arc basin-related boninites occur in close association to broadly back arc basin basalt (BABB) with various subduction zone signature (from N-MORB, E-MORB, transitional MORB-IAT to IAT); (2) fore-arc extension-related boninites are dominated by low-Ca boninites, whereas back-arc basin-related boninites on the whole display high-Ca boninite characteristics with relatively lower SiO_2 and Na_2O and lack obvious L-MREE and Zr–Hf enrichment (Crawford et al., 1989). These observations reflect their potentially significant differences in P-T conditions and chemical compositions of slab-derived components (including fluids and probably a hydrous melt phase) from fore-arc extension-related boninites. However, a better knowledge of boninite-related magmatic evolution and its geodynamic implications is hampered by a limited number of modern boninite localities. In addition, the exact temporal and spatial relationship between boninite and coexisting volcanic rocks such as island arc tholeiites (IAT) and back-arc basin basalts (BABB), is difficult to determine at present (Crawford and Keays, 1987; Portnyagin et al., 1997).

The North Qilian Orogenic belt is a typical oceanic suture zone with a western Pacific-type subduction history that consists of ophiolitic fragments, high-pressure/low-temperature (HP/LT) metamorphic rocks, arc magmatic sequences including volcanic rocks and I-type granite/granodiotrite plutons. (e.g., Xiao et al., 1978; Wu et al., 1993; Feng and He, 1995; Zhang et al., 1997; Qian et al., 2001; Xia et al., 2003; Smith and Yang, 2006; Song et al., 2006; Tseng et al., 2007; Zhang et al., 2007; Song et al., 2009a, 2009b; Xia and Song, 2010). Studies of spatially coexisting HP/LT metamorphic rocks concur with the notion of fossil arc-back-arc basic framework, and emphasize the presence of a once stable, cold oceanic subduction zone with a low geothermal gradient (6–7 °C/km) at 490–440 Ma (Wu et al., 1993; Song et al., 2004; Song et al., 2006; Song et al., 2007; Zhang et al., 2007; Song et al., 2009b). Here, we present an integrated study of petrology, geochemistry and geochronology for the Dachadaban (DCDB) tholeiite–boninite terrane. The lithological succession and ages of these rocks provide important clues on subduction zone magmatic evolution with continued asthenospheric upwelling and mantle wedge hydration from subduction initiation

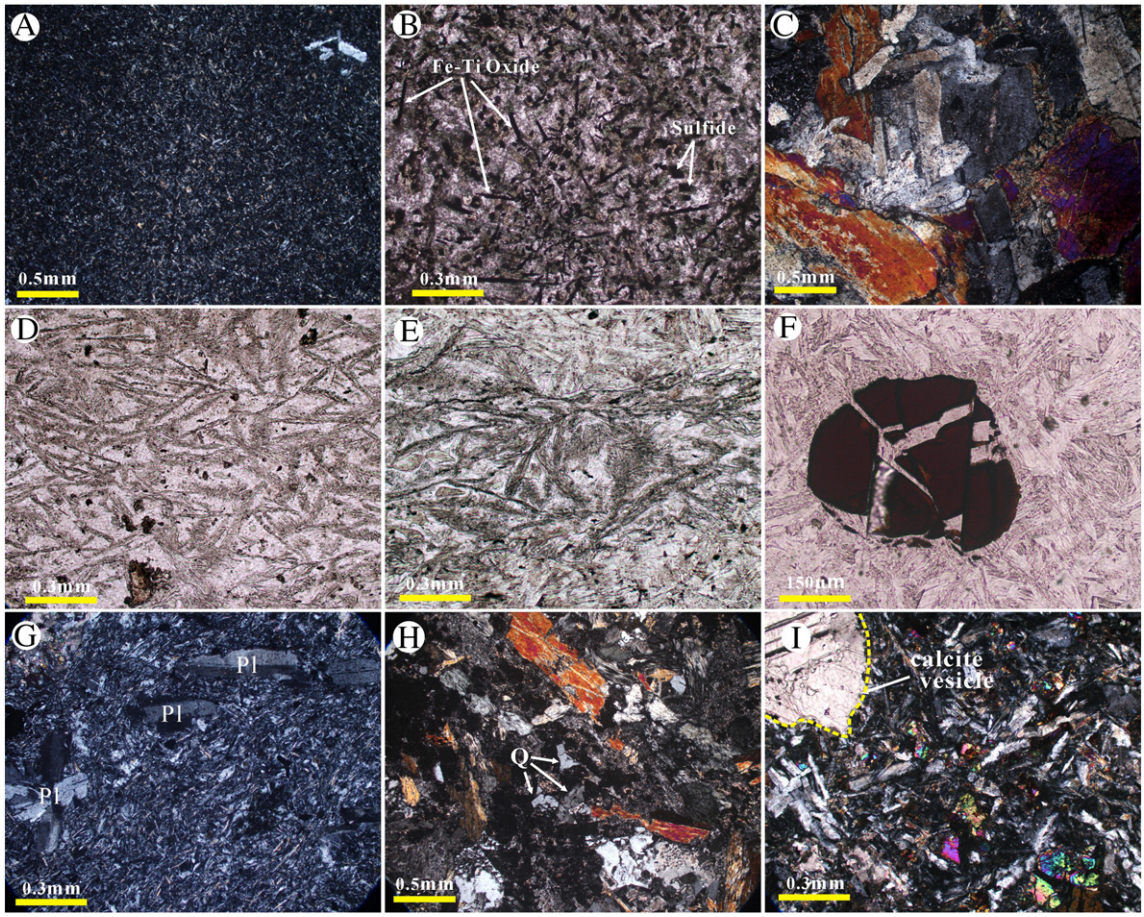

Fig. 3. Microphotographs showing textures of the DCDB tholeiite–boninite terrane. A: Aphyric texture in the lower tholeiites (4SD02). B: Acicular Fe–Ti-oxides in E-MORB-like sample (2SD27) from lower tholeiite unit. C: Gabbro sample (08QS72) from lower tholeiite unit. D–E: Holohyaline and hyalopilitic basaltandesite from upper boninite unit (08QS71). F: Reddish brown Cr-spinel as isolated euhedral rhombus in upper boninitic sample (08QS71). G: Plagioclase phenocrysts in highly evolved lava sample (08QS64). H: Quartz gabbro in upper boninitic unit (2SD15). I: Vesicles or amygdales in dolerite dyke margins from upper lava unit (08QS68).

to the subsequent back-arc spreading. A statistical analysis on global boninite terranes reveals a first-order intrinsic link between light rare earth element (LREE) and Zr–Hf enrichment. We find that the distance from the magma source region to the subducting slab (or trench) may be the major cause of the boninite LREE-Zr enrichment array.

2. Geological setting

The North Qilian orogenic belt (NQOB) is located at the northern margin of the Tibetan plateau (Fig. 1A). It extends in NW-SE direction for 1000 km between the Alashan block and the Qilian-Qaidam micro-continent and is offset by the Altyn Tagh Fault, the largest sinistral strike-slip fault in western China (Fig. 1B). The middle sector of NQOB is a well-studied region and consists of three major tectono-stratigraphic units (Zhang et al., 1997; Song et al., 2004; Wang et al., 2005; Song et al., 2006; Song et al., 2007; Zhang et al., 2007): 1) the South ophiolite belt, 2) the North back-arc basin ophiolite-volcanic belt, which is conformably overlain by a Silurian flysch formation, and 3) a sandwiched arc magmatic complex intercalated with slices of high-pressure metamorphic (HPM) rocks (Fig. 1B–C).

The South ophiolite belt consists mainly of mafic-ultramafic fragments and deep seawater clastic rocks, and has been interpreted as mixture of ocean crust fragments and trench-facies sedimentary rocks of the ancient Qilian Ocean (Xiao et al., 1978; Feng and He, 1995; Zhang et al., 1997). Two well-preserved ophiolite suites (Yushigou and Dongcaohe ophiolite) that consist of mantle peridotites, ultramafic-mafic cumulates (dunite, troctolite and gabbro), pillow lavas and radiolarian cherts are exposed within this belt (Xiao et al., 1978; Feng and He, 1995; Song and Su, 1998; Hou et al., 2006; Song et al., 2009b). Zircon dating by SHRIMP of the gabbros closely related to pillow lavas yield an age of 550 ± 17 Ma and 497 ± 7 Ma (Shi et al., 2004; Tseng et al., 2007), respectively (Fig. 1C).

The northern ophiolite belt is located to the north of the arc-magmatic complex belt (Fig. 1C). Basaltic rocks in this belt include N-type MORB and IAB. In this sequence are abundant mafic breccias, arc-derived volcanic and volcaniclastic rocks, and continent-derived sedimentary, suggesting a back-arc or marginal basin setting (Zhang et al., 1997; Qian et al., 2001; Xia and Song, 2010).

The arc magmatic belt consists predominantly of calc-alkaline intermediate-felsic volcanic and volcaniclastic rocks, as well as I-type granite/granodiorite plutons, with emplacement ages ranging from 516 to 446 Ma (Zhang et al., 1997; Wang et al., 2005; Wu et al., 2010). The HP/LT metamorphic rocks occur as three fault-bound slices within the arc-magmatic complex (Fig. 1C). They are mainly composed of blueschist- to eclogite-facies meta-greywacke, meta-pelite, meta-chert with blocks of mafic blueschist, low-T eclogite, marble and serpentinized peridotite (Wu et al., 1993; Song et al., 2007, 2009a). Recent findings of lawsonite-bearing eclogite and carpholite-bearing meta-pelite present convincing evidence for a cold oceanic lithosphere subduction zone with low geothermal gradient (6–7 °C/km) in the early Paleozoic (Song et al., 2007; Zhang et al., 2007). Zircon SHRIMP dating indicates that the eclogite-facies metamorphism occurred between ca. 490 and 460 Ma (Song et al., 2004,

Table 1
Representative compositions of spinel phenocrysts and inclusions trapped in Mg-phase found in DCDB massif.

	Sample no.	SiO_2	TiO_2	Al_2O_3	FeO*	MnO	MgO	Cr_2O_3	NiO	Total	Cr#	Mg#
I	4SD02-1	0.07	1.02	22.91	22.60	0.21	13.21	38.89	0.12	99.03	0.53	0.59
	4SD02-3	0.06	0.95	22.69	22.95	0.25	12.86	39.07	0.14	98.97	0.54	0.58
	4SD02-4	0.06	0.92	22.70	23.97	0.23	12.03	39.07	0.07	99.05	0.54	0.55
	4SD02-5	0.07	0.97	22.64	22.64	0.22	13.54	38.81	0.12	99.01	0.53	0.61
	4SD09-2	0.04	0.34	25.90	20.96	0.27	11.96	39.46	0.12	99.05	0.51	0.55
	4SD07-2	0.05	0.96	24.64	21.47	0.13	14.18	37.49	0.13	99.05	0.51	0.63
II	2SD03-3	0.07	0.18	10.85	18.56	0.58	12.77	56.80	0.03	99.84	0.78	0.62
	2SD03-4	0.09	0.34	11.93	21.83	0.98	9.87	53.40	0.10	98.54	0.75	0.49
	4SD10-2	0.12	0.24	9.32	17.24	0.34	14.74	57.85	0.09	99.94	0.81	0.70
	4SD10-4	0.06	0.24	8.06	16.80	0.48	14.29	59.65	0.07	99.65	0.83	0.69
	4SD11-2	0.04	0.21	10.17	19.27	0.58	12.35	57.93	0.00	100.55	0.79	0.60
	4SD11-6	0.03	0.24	10.17	19.57	0.52	11.96	57.19	0.00	99.68	0.79	0.58
	4SD13-2	0.05	0.11	9.82	14.92	0.47	15.13	60.13	0.09	100.72	0.80	0.71
	4SD13-1	0.09	0.21	10.09	14.94	0.50	15.65	58.81	0.13	100.42	0.80	0.74
	4SD15-1	0.10	0.22	10.38	16.54	0.49	13.79	58.59	0.06	100.17	0.79	0.66
	4SD15-3	0.06	0.29	11.60	16.23	0.50	14.77	56.69	0.09	100.23	0.77	0.70
	4SD17-1	0.02	0.25	10.46	14.30	0.45	15.63	60.21	0.22	101.54	0.79	0.73
	4SD17-2	0.04	0.28	10.37	14.45	0.43	15.46	58.48	0.13	99.64	0.79	0.73
	4SD18-2	0.02	0.22	10.66	14.84	0.42	14.84	59.84	0.21	101.05	0.79	0.70
	4SD18-4	0.07	0.25	9.87	16.85	0.52	14.42	58.15	0.05	100.18	0.80	0.69
	4SD23-2	0.04	0.22	11.28	17.15	1.03	12.41	58.21	0.16	100.50	0.78	0.60
	4SD23-5	0.08	0.29	10.75	19.66	0.53	11.32	56.78	0.00	99.41	0.78	0.56
	08QS61-5	0.04	0.19	9.86	17.10	0.98	12.82	59.55	0.24	100.78	0.80	0.63
	08QS61-6	0.06	0.15	9.47	16.78	0.54	13.41	59.15	0.10	99.66	0.81	0.65
	08QS70-1	0.13	0.28	9.19	15.58	0.39	14.52	59.87	0.12	100.08	0.81	0.71
	08QS70-4	0.05	0.23	10.16	13.94	0.55	15.18	60.25	0.16	100.52	0.80	0.72
	08QS71-1	0.05	0.21	10.49	14.34	0.52	15.63	59.18	0.15	100.57	0.79	0.74
	08QS71-9	0.05	0.21	11.21	15.70	0.54	12.87	59.27	0.10	99.95	0.78	0.62
III	9SD04-1	0.07	0.22	9.69	23.81	0.34	9.60	55.10	0.14	98.97	0.79	0.48
	9SD04-2	0.06	0.15	9.57	23.68	0.28	9.96	55.15	0.06	98.91	0.79	0.50
	9SD05-1	0.04	0.19	10.22	24.46	0.33	8.98	54.71	0.14	99.07	0.78	0.45
	9SD05-2	0.07	0.11	9.13	27.25	0.36	7.93	54.06	0.09	99.00	0.80	0.40
	9SD06-1	0.00	0.23	10.53	24.00	0.29	9.51	54.38	0.00	98.94	0.78	0.48
	9SD06-2	0.07	0.19	10.44	22.83	0.33	10.15	54.91	0.07	98.99	0.78	0.51
	9SD08-1	0.05	0.21	10.02	20.93	0.24	11.06	56.49	0.07	99.07	0.79	0.55
	9SD08-2	0.10	0.22	9.88	23.60	0.31	8.72	56.03	0.10	98.96	0.79	0.44
	9SD10-1	0.12	0.17	9.59	23.43	0.32	9.13	56.14	0.09	98.99	0.80	0.46
	9SD10-2	0.09	0.24	8.72	25.27	0.31	8.41	55.91	0.03	98.98	0.81	0.42

FeO* = total iron as FeO. Cr# = Cr/(Cr + Al); Mg# = Mg/ (Mg + Fe). I, samples from the lower tholeiitic unit; II, upper boninite pillow lava; III, quartz gabbros associated with upper lava.

2006; Zhang et al., 2007). $^{40}Ar/^{39}Ar$ ages of phengite and glaucophane from blueschist samples range between 460 and 440 Ma (e.g., Wu et al., 1993; Zhang et al., 1997; Liu et al., 2006). Therefore, these subduction-related HP metamorphic ages (489–440 Ma) are generally coupled with that of the arc magmatic activity (520–446 Ma).

3. Field occurrence, petrography and mineral chemistry

The DCDB tholeiite–boninite terrane is ~4.5 km thick and is uncomfortably overlain by Devonian Molasses (Fig. 2D). It is separated by a post-Devonian sedimentary cover from the ophiolite belt with a back-arc basin origin to the north and overthrusted onto an arc-magmatic complex belt to the south (Fig. 1C). The DCDB tholeiite–boninite terrane was first documented as a typical Penrose-type ophiolite sequence by Feng and He (1995) and then reinterpreted as boninites by Chen et al. (1995) and Zhang et al. (1998) based on major and trace element geochemistry.

3.1. Lower tholeiite unit

The lower tholeiite unit is ~1 km thick and is predominantly composed of massive lava flows with columnar joints, subordinate dolerite dykes and gabbro intrusions (up to 100 m in width). Lavas and dykes are generally aphyric with locally embayed plagioclase phenocrysts and pyroxene pseudomorphs in either a subophitic- to intergranular groundmass or in a groundmass of devitrified glass (Fig. 3A). Fe–Ti oxide is a ubiquitous accessory phase (Fig. 3B). Locally sulfide mineralization resembles that in the upper boninite unit.

3.2. Upper boninite unit

The upper boninite unit is ~3.5 km thick and conformably overlies the lower tholeiite unit (Fig. 2). There are no other volcanic/sedimentary sequences or large fault between these two units, thus suggesting a continuum in the volcanic activity. The upper boninite unit is composed predominantly of well-developed pillow lavas, diabase dykes and gabbroic sills. Pillows (Fig. 2B) are mostly ~0.5–1.0 m in size with abundant vesicles gradually concentrated outward, forming a concentric zone in outmost glassy margin (Fig. 2B). These vesicle zones are much thicker (6–10 cm) than that of common mid-ocean-ridge pillow lavas (0.5–1 cm) (Moore, 1970; Moore and Schilling, 1973; Moore, 1975; Kennish and Lutz, 1998), indicating high initial volatile contents in their parental magmas and eruption in relatively shallow water. The lack of pelagic or volcaniclastic sediments between pillows suggests rapid volcanic eruption. Intrusive rocks constitute a significant proportion (~10%) in the upper boninitic unit, occurring either as diabase dikes (0.5–1 m wide) (Fig. 2C) or as sills (up to 50–100 m thick) of quartz-bearing gabbro.

The boninitic extrusive rocks are phenocryst-poor with glassy textures including microlites. In weakly altered samples, acicular, skeletal pyroxene with feathery terminations and spinifex-like pseudomorphs of olivine microlites are randomly oriented and set in a groundmass of altered glass matrix (Fig. 3D–E). This spinifex-like texture probably reflects rapid cooling and olivine/orthopyroxene nucleation. Only 6 of the 30 lava samples have a few phenocrysts (up to 1–2%). Plagioclase or quart phenocrysts are only observed in relatively evolved samples (SiO_2 > 58 wt.%) (Fig. 3G). The dyke samples are aphyric and locally vesicular and show mainly a sub-ophitic to intergranular texture; devitrified glass and small anhedral pyroxene grains in a network of lath-shaped plagioclase microphenocrysts (Fig. 3H–I). Quartz-bearing gabbroic intrusions have a medium- to coarse-grained texture with mineral assemblage of augite, plagioclase and quartz (up to 10%) (Fig. 3H).

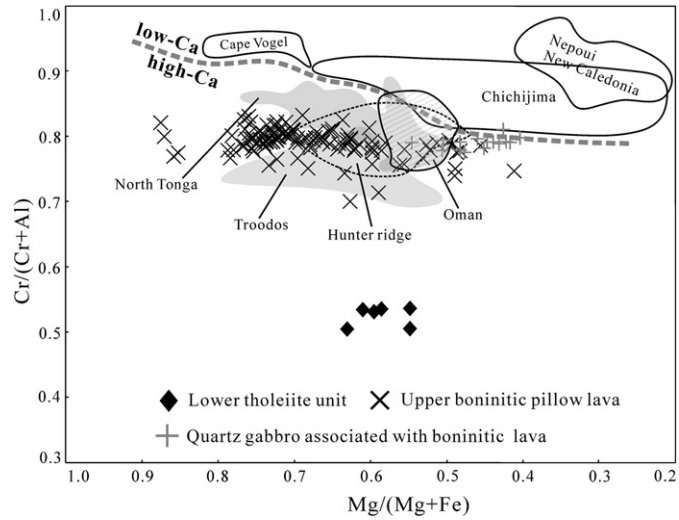

Fig. 4. Chemical comparison of spinel from DCDB boninites with typical high-Ca boninites and low-Ca boninites. The thick dotted line shows the boundary between typical high-Ca and low-Ca boninites. Data sources are for Troodos, Duncan and Green (1987); Thy and Xenophontos (1991); Bednarz and Schmincke (1994); for North Tonga, Sobolev and Danyushevsky (1994); Danyushevsky et al. (1995); for Hunter Ridge, Sigurdsson et al. (2003); for Oman, Ishikawa et al. (2002); for Cape Vogel, Walker and Cameron (1983); Kamenetsky et al. (2002); for Nepoui, New Caledonia, Sameshima et al. (1983); for Chichijima, Umino (1986) and Taylor (1992).

3.3. Spinel mineral chemistry

As a highly refractory and resistant phase, spinel from terrestrial mafic and ultramafic rocks has been demonstrated to be an effective "petrogenetic indicator" that retains information about the primary liquid compositions characteristic of tectonic settings (e.g., Dick and Bullen, 1984; Duncan and Green, 1987; Ariskin and Nikolaev, 1996; Barnes and Roeder, 2001; Poustovetov and Roeder, 2001). Spinels were analyzed using a JEOL JXA-8100 wavelength dispersive electron microprobe at Peking University. The operating conditions were 15 kV acceleration voltages with 10 nA beam current and a beam diameter of 1 μm. Ferric iron in spinels was calculated according to the charge balance equation (Droop, 1978).

In the DCDB boninite terrane, Cr-spinel occurs as reddish brown, isolated euhedral crystals that are mainly restricted to MgO-rich lava samples in the upper boninite unit (Fig. 3F). Representative compositions are given in Table 1. Spinels from the boninitic pillow lavas

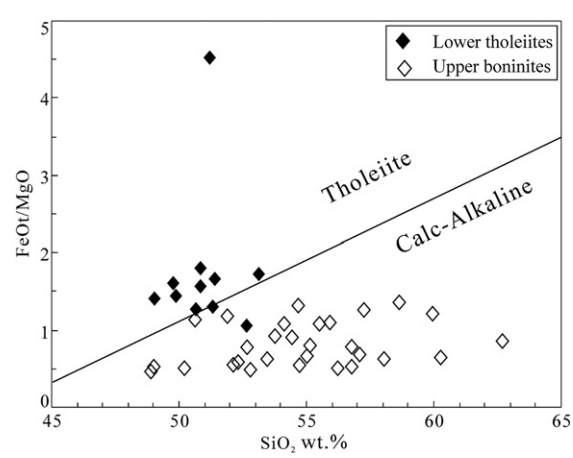

Fig. 5. Plot of SiO_2 vs. FeOT/MgO for DCDB boninite terrane. The boundary line between tholeiitic and calc-alkaline rock types is from Miyashiro (1974).

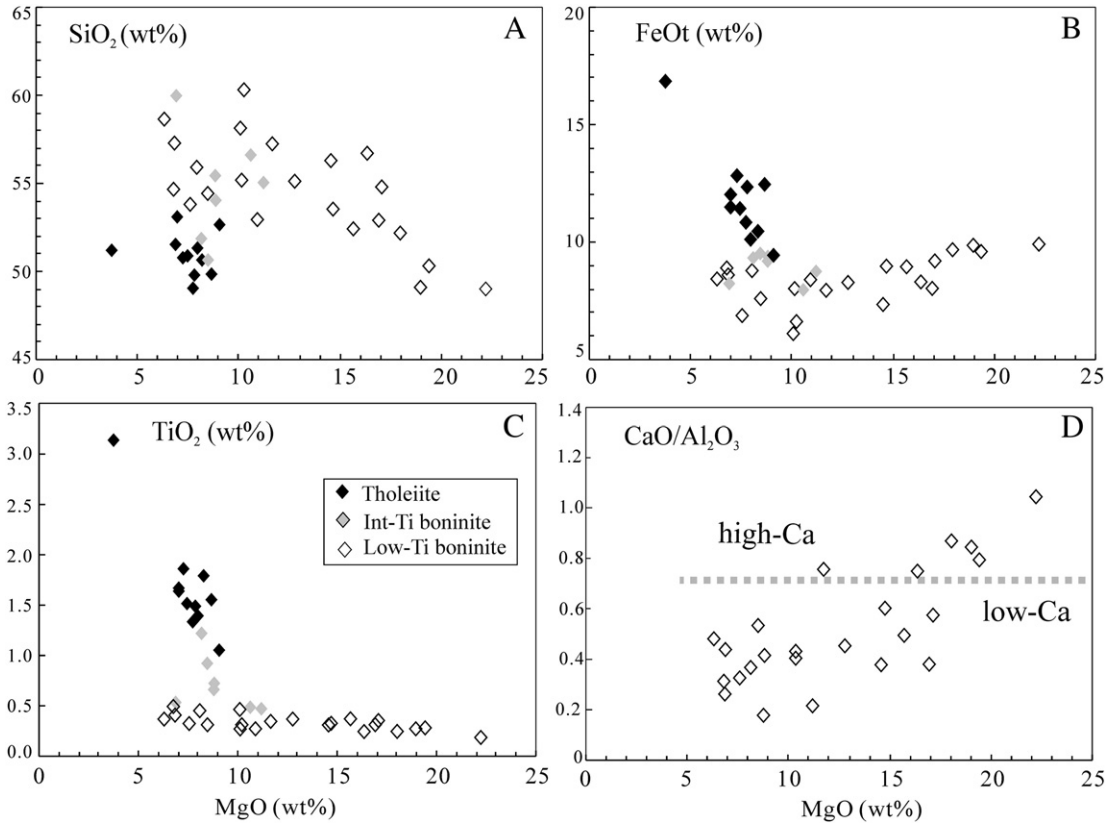

Fig. 6. A–C: Bowen diagrams showing correlations between MgO and other major elements of all rocks from the DCDB tholeiite–boninite terrane (A–C). D: plot of CaO/Al_2O vs. MgO for DCDB upper boninites. The thick dotted line shows the boundary between high-Ca and low-Ca boninites according to definition from Crawford et al. (1989).

have very high Cr_2O_3 (mainly 56–61 wt.%), and low Al_2O_3 (mainly 9–11 wt.%) and TiO_2 (0.1–0.34 wt.%) with high $Cr^{\#}$ [$100\times Cr/(Cr+Al)=78$–82], high $Mg^{\#}$ [$100\times Mg/(Mg+Fe^{2+})=41$–88] and low $Fe^{\#}$ [$100\times Fe^{3+}/(Fe^{3+}+Cr+Al)=4$–7], which reflect primitive characteristics of the boninitic pillow lavas. Spinel compositions from the DCDB boninites overlaps the high-Ca boninite fields defined by those from North Tonga (Sobolev and Danyushevsky, 1994; Danyushevsky et al., 1995), Troodos (Duncan and Green, 1987; Thy and Xenophontos, 1991; Bednarz and Schmincke, 1994), Hunter Ridge (Sigurdsson et al., 2003) and Oman ophiolite (Ishikawa et al., 2002) (Fig. 4). Cr-rich spinels are also present in intrusive rocks of the upper boninite unit. Comparing to the lava samples, spinels from quartz gabbroic intrusions display a similar level of Cr_2O_3 (54–57 wt.%), Al_2O_3 (9–11 wt.%), TiO_2 (0.11–0.28 wt.%) and $Cr^{\#}$ (78–81), but high FeOt (21–27 wt.%), low MgO (8–11 wt.%) and thus low Mg# (40–55) (Fig. 4). This is consistent with their highly evolved composition.

4. Whole-rock geochemistry

Samples for whole-rock geochemical analyses were carefully selected from the least altered and metamorphosed interiors of pillow lavas or dykes. Fine calcite veins and any altered surfaces were removed before grinding into powders in an agate mortar. Bulk-rock major element oxide analyses were done on a Leeman Prodigy inductively coupled plasma-optical emission spectroscopy (ICP-OES) and trace elements on an Agilent-7500a inductively coupled plasma mass spectrometry (ICP-MS) at China University of Geosciences, Beijing. Detailed descriptions of sample preparation and analytical procedures are given in Song et al. (2010).

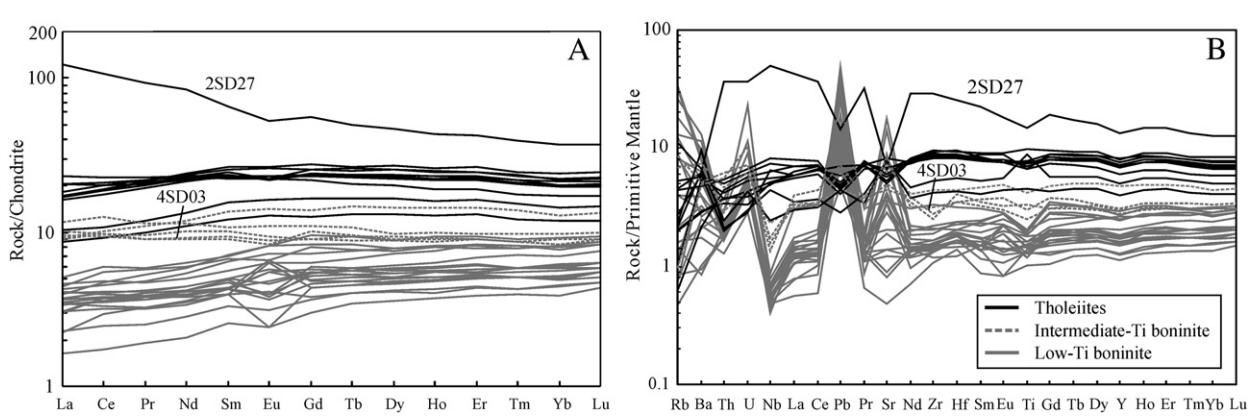

Fig. 7. Chondrite-normalized REE (A) and Primitive mantle-normalized multi-element diagrams (B) for the DCDB tholeiite-boninite terrane. Normalizing values are from Sun and McDonough (1989).

Table 2
Major and trace element compositions of the DCDB tholeiite–boninite terrane, North Qilian.

Sample	4SD02	4SD03	4SD04	4SD05	4SD06	4SD07	4SD22	4SD27	2SD27	2SD29	2SD31	08QS72	S4SD09	4SD09-2	4SD10	4SD11	4SD13	4SD15	4SD16
Unit	L	L	L	L	L	L	L	L	L	L	L	L	U	U	U	U	U	U	U
Rock type	ML	D	D	ML	ML	ML	ML	ML	ML	ML	ML	G	G	G	PL	PL	PL	PL	D
SiO_2	53.11	59.92	49.04	50.85	49.9	51.32	50.67	49.73	51.18	51.38	50.82	52.65	51.92	50.69	58.1	53.78	52.15	52.83	55.95
TiO_2	1.64	0.54	1.33	1.51	1.56	1.39	1.79	1.47	3.14	1.66	1.86	1.05	1.22	0.93	0.26	0.32	0.24	0.30	0.44
Al_2O_3	13.27	14.90	15.89	14.20	14.4	14.46	14.40	14.53	12.41	14.15	13.53	13.12	14.34	15.23	11.52	15.70	10.55	13.42	15.11
Fe_2O_3t	12.02	8.27	10.81	11.45	12.47	10.11	10.44	12.34	16.85	11.49	12.87	9.38	9.41	9.52	6.08	6.82	9.64	8.01	8.76
MnO	0.17	0.12	0.13	0.19	0.19	0.16	0.12	0.18	0.24	0.18	0.23	0.13	0.11	0.14	0.11	0.13	0.17	0.14	0.14
MgO	7.01	6.87	7.72	7.42	8.67	7.96	8.25	7.81	3.77	7.00	7.30	9.07	8.14	8.45	10.13	7.61	18.03	16.94	8.09
CaO	7.89	3.92	12.28	10.82	9.69	10.41	10.87	10.36	7.50	10.89	10.07	11.29	11.81	11.72	11.10	7.29	9.19	4.98	5.55
Na_2O	4.70	5.35	2.46	3.32	2.88	3.84	3.12	3.03	3.78	2.93	3.07	2.93	2.90	2.84	2.59	8.15	0.01	3.34	5.91
K_2O	0.04	0.04	0.22	0.10	0.10	0.20	0.20	0.36	0.53	0.16	0.10	0.30	0.07	0.42	0.02	0.18	0.01	0.01	0.04
P_2O_5	0.14	0.06	0.14	0.14	0.14	0.14	0.15	0.20	0.54	0.14	0.15	0.07	0.09	0.06	0.03	0.02	0.02	0.03	0.02
Mg#	57.6	65.9	62.5	60.2	61.8	64.7	64.8	59.6	34.3	58.7	56.9	69.3	66.8	67.4	79.5	72.2	81.3	83.1	68.3
Trace elements (ppm)																			
Sc	42.68	36.15	43.72	43.12	44.07	37.9	43.72	44.54	30.58	42.98	43.68	41.94	–	42.36	22.84	32.14	29.11	–	39.28
Ti	10178	3250	9256	9896	9598	8650	11664	8784	19374	9712	12643	5936	–	5404	1677	2096	1893	–	2666
V	356	249	359	329	344	275	377	311	251	349	409	294	–	266.20	134.74	182.62	178.26	–	223.00
Cr	157.18	59.06	274.60	263.80	225.37	325.60	220.40	218.60	5.28	125.66	63.90	250.00	–	247.00	433.40	573.60	734.10	–	220.40
Mn	1295.80	887.91	1090.40	1383.60	1346.96	1098.8	890.40	1357.00	1796.2	1353.20	1753.23	1036.00	–	1044.00	693.00	922.80	1208.87	–	945.60
Co	48.44	27.40	51.44	48.18	47.93	40.38	48.56	43.00	33.44	44.18	50.92	43.60	–	38.80	29.78	33.94	42.52	–	33.54
Ni	63.28	29.88	94.80	78.72	74.91	109.02	80.30	77.46	4.01	55.70	47.20	79.46	–	80.10	116.74	150.00	276.73	–	64.10
Cu	5.94	214.20	21.38	96.34	59.78	18.95	24.32	61.14	33.56	29.60	75.82	9.18	–	9.678	93.54	39.44	4.64	–	80.70
Zn	49.32	46.37	22.26	57.90	70.31	39.72	31.10	65.39	108.28	60.78	95.17	39.48	–	40.59	40.8	47.52	59.49	–	51.60
Ga	16.75	13.15	20.92	17.05	19.89	16.5	16.17	17.67	23.34	17.67	18.46	15.06	–	13.47	6.83	11.54	8.53	–	12.59
Rb	0.65	0.62	0.40	3.38	1.28	2.78	1.72	1.26	1.35	2.87	1.47	7.06	–	7.049	1.00	7.79	0.91	–	0.74
Sr	106.80	177.02	172.60	139.88	144.98	125.90	165.78	126.10	147.46	120.32	112.17	170.24	–	152.70	105.70	88.38	73.98	–	300.80
Y	34.46	12.58	31.10	31.50	32.09	27.26	22.70	37.04	61.40	32.58	36.57	18.30	–	21.58	5.66	11.93	6.74	–	11.42
Zr	105.06	35.27	92.08	100.58	96.40	100.94	59.00	94.66	321.80	98.92	106.60	46.48	–	49.34	17.50	18.47	17.28	–	21.26
Nb	3.99	1.13	4.57	5.29	3.62	5.82	3.18	3.47	35.86	3.71	4.63	1.74	–	1.67	0.47	0.50	0.46	–	0.48
Cs	0.14	0.10	0.14	0.20	0.12	0.14	0.09	0.13	0.41	0.33	0.19	0.22	–	0.22	0.57	1.42	0.26	–	0.12
Ba	38.44	34.68	14.84	39.96	20.38	33.78	41.72	19.83	44.84	43.48	67.05	47.18	–	46.26	14.52	36.84	5.94	–	35.68
La	4.07	2.28	4.89	4.89	3.82	5.51	2.43	4.304	29.12	4.02	4.00	2.05	–	2.18	0.87	1.10	0.82	–	1.01
Ce	11.71	5.76	12.42	12.83	10.79	13.79	6.54	12.33	65.66	11.43	11.69	5.63	–	6.19	2.34	2.92	2.02	–	2.79
Pr	1.98	0.85	1.97	2.06	1.83	2.14	1.13	2.076	8.80	1.92	2.01	0.95	–	1.04	0.36	0.45	0.31	–	0.46
Nd	10.68	4.27	10.22	10.75	9.91	10.77	6.28	10.93	39.08	10.38	11.23	5.11	–	5.54	1.79	2.32	1.64	–	2.51
Sm	3.77	1.43	3.44	3.60	3.53	3.42	2.37	3.89	10.03	3.62	4.05	1.84	–	2.06	0.61	0.86	0.6	–	0.99
Eu	1.28	0.51	1.35	1.26	1.34	1.29	0.93	1.50	3.06	1.27	1.54	0.74	–	0.81	0.24	0.37	0.37	–	0.42
Gd	5.22	1.85	4.74	4.82	4.80	4.45	3.42	5.24	11.57	4.96	5.66	2.60	–	2.85	0.78	1.29	0.89	–	1.48
Tb	0.94	0.33	0.85	0.87	0.86	0.77	0.62	0.96	1.85	0.88	1.00	0.49	–	0.55	0.15	0.25	0.17	–	0.28
Dy	6.43	2.24	5.69	5.89	5.81	5.10	4.24	6.44	11.86	6.04	6.86	3.31	–	3.68	1.04	1.85	1.18	–	1.98
Ho	1.38	0.49	1.23	1.26	1.25	1.08	0.91	1.42	2.44	1.30	1.48	0.73	–	0.81	0.23	0.43	0.27	–	0.45
Er	4.09	1.48	3.61	3.75	3.69	3.15	2.68	4.08	7.06	3.86	4.38	2.16	–	2.37	0.72	1.37	0.82	–	1.38
Tm	0.59	0.22	0.52	0.55	0.53	0.45	0.39	0.60	1.00	0.56	0.63	0.31	–	0.35	0.11	0.21	0.13	–	0.21
Yb	3.80	1.41	3.33	3.43	3.39	2.91	2.46	3.70	6.24	3.60	4.10	2.01	–	2.19	0.76	1.35	0.85	–	1.31
Lu	0.58	0.22	0.50	0.52	0.51	0.44	0.38	0.57	0.94	0.54	0.62	0.30	–	0.34	0.12	0.21	0.14	–	0.21
Hf	2.94	1.08	2.51	2.74	2.58	2.61	1.71	2.56	7.90	2.7	2.88	1.33	–	1.36	0.57	0.63	0.56	–	0.74
Ta	0.46	0.25	0.48	0.48	0.34	0.56	0.28	0.19	2.41	0.27	0.33	0.21	–	0.15	0.07	0.12	0.11	–	0.10
Pb	0.35	1.74	0.31	0.33	0.29	0.32	0.20	0.37	1.04	0.42	0.50	0.31	–	0.32	2.13	1.81	0.91	–	2.57
Th	0.36	0.48	0.38	0.43	0.29	0.46	0.17	0.32	3.09	0.31	0.18	0.21	–	0.25	0.24	0.18	0.18	–	0.17
U	0.11	0.22	0.12	0.13	0.07	0.14	0.06	0.08	0.77	0.09	0.06	0.09	–	0.09	0.48	0.11	0.1	–	0.11

L, Lower tholeiitic unit; U, Upper boninitic unit; ML, massive lava; D, Dolerite; G, gabbro; PL, pillow lava; All major elements have been renormalized to 100 wt.% anhydrous.

Table 2 (*continued*)

Sample	4SD17	4SD18	4SD20	4SD21	4SD23	2SD03	S2SD06	2SD09	2SD11	2SD18	2SD19	2SD20	2SD23	2SD25	2SD26	08QS62	08QS64	08QS70	08QS71
Unit	U	U	U	U	U	U	U	U	U	U	U	U	U	U	U	U	U	U	U
Rock type	PL	PL	G	G	PL	PL	PL	Q-G	PL	D	PL	PL	D	D	PL	PL	PL	PL	PL
SiO_2	56.27	56.82	54.74	57.13	55.08	60.29	52.7	54.43	57.26	55.57	53.47	52.36	54.7	55.18	55.17	49.03	58.65	50.26	48.93
TiO_2	0.31	0.24	0.35	0.33	0.36	0.30	0.26	0.31	0.40	0.70	0.32	0.36	0.49	0.50	0.46	0.27	0.36	0.28	0.18
Al_2O_3	12.72	9.98	11.19	12.22	13.19	12.26	11.24	16.93	15.46	15.54	12.04	12.51	16.54	16.54	14.71	11.09	13.15	10.8	8.76
Fe_2O_3t	7.30	8.26	9.17	7.89	8.25	6.55	8.42	7.58	8.58	9.39	8.94	8.92	8.85	8.75	7.96	9.85	8.41	9.59	9.9
MnO	0.13	0.16	0.16	0.13	0.11	0.10	0.18	0.14	0.12	0.12	0.17	0.14	0.12	0.12	0.14	0.17	0.10	0.16	0.18
MgO	14.58	16.39	17.13	11.72	12.79	10.27	10.93	8.50	6.88	8.83	14.76	15.71	6.81	11.16	10.19	19.00	6.33	19.44	22.23
CaO	4.74	7.45	6.41	9.24	5.95	5.15	13.31	9.03	6.76	6.39	7.26	6.15	5.12	3.6	5.85	9.38	6.31	8.54	9.16
Na_2O	3.93	0.13	0.19	0.86	4.18	4.96	2.80	2.64	4.46	2.71	2.51	3.77	7.31	3.93	5.34	0.63	6.63	0.90	0.60
K_2O	0.01	0.55	0.65	0.43	0.07	0.11	0.13	0.43	0.06	0.67	0.52	0.05	0.03	0.17	0.16	0.55	0.05	0.01	0.05
P_2O_5	0.01	0.01	0.02	0.03	0.03	0.01	0.02	0.02	0.03	0.08	0.02	0.02	0.04	0.05	0.03	0.03	0.03	0.02	0.01
Mg#	82.3	82.2	81.3	77.6	78.3	78.5	75.2	72.3	65.1	68.7	79.4	80.4	64.2	74.8	74.9	81.8	63.7	82.5	84.0
Trace elements (ppm)																			
Sc	32.28	27.96	39.00	46.85	–	29.54	32.33	35.77	32.96	36.84	36.7	35.67	36.28	37.27	34.86	32.84	29.24	29	24.81
Ti	1999	1666	1730	2345	–	1810	1538	1524.4	2369	3954	1922.3	1888	2397	2677	2512	1725	2090	1865	1326
V	162.92	184.50	182.85	237.16	–	154.72	193.80	172.30	257.70	247.60	209.10	176.40	210.30	233.60	202.70	208.22	167.16	175.32	167.94
Cr	1250.40	806.40	1121.51	606.58	–	335.00	742.10	229.20	221.80	437.70	901.70	871.30	47.94	92.55	424.80	692.98	345.40	1241.40	1125.98
Mn	1047.40	1194.96	1173.54	941.78	–	748.20	1109.30	950.80	845.70	858.70	1307.60	971.30	831.40	781.30	1008.50	1193.58	640.20	1108.40	1293.21
Co	59.26	52.64	48.00	38.61	–	27.66	49.40	54.61	66.41	46.75	62.63	60.30	71.58	40.76	46.83	53.74	29.12	57.28	62.39
Ni	413.80	292.98	214.17	114.51	–	80.14	212.50	106.50	111.20	195.30	336.60	314.60	38.61	71.41	108.1	268.92	91.80	411.60	417.18
Cu	2.74	4.58	3.17	4.12	–	50.68	21.04	5.28	3.24	2.62	9.89	9.29	110.50	2.56	61.77	26.03	13.00	2.88	2.13
Zn	66.16	68.60	61.70	26.84	–	40.94	46.06	27.37	23.14	24.07	70.53	49.36	40.48	42.40	50.55	61.11	45.22	58.14	70.42
Ga	9.91	8.67	9.46	10.18	–	6.23	8.96	13.09	14.07	13.12	9.34	7.54	12.42	13.06	11.30	9.17	7.42	8.81	8.25
Rb	0.30	5.25	16.47	5.38	–	1.35	21.67	11.60	2.50	5.42	8.37	0.48	0.48	5.79	2.52	20.44	0.89	0.54	1.04
Sr	29.28	39.70	17.06	70.04	–	25.52	187.4	186.9	142.2	93.26	18.83	29.11	374.4	76.34	43.16	73.02	81.24	60.26	10.28
Y	8.07	7.45	6.92	8.44	–	6.81	8.07	7.81	11.18	14.1	7.97	6.97	11.44	12.42	13.15	5.81	9.19	7.10	5.10
Zr	16.73	15.30	15.51	17.17	–	14.93	15.8	13.19	23.28	31.35	16.55	16.68	22.92	37.09	24.50	14.88	18.43	16.95	11.98
Nb	0.46	0.40	0.48	0.50	–	0.40	0.32	0.35	0.56	0.97	0.38	0.35	0.47	0.62	0.29	0.42	0.45	0.43	0.34
Cs	0.23	0.28	1.00	0.67	–	0.19	–	–	–	–	–	–	–	–	–	0.61	0.07	0.21	0.32
Ba	7.18	43.77	90.49	27.58	–	22.9	59.95	69.05	21.01	36.04	79.47	17.49	37.11	18.22	27.51	54.03	15.21	6.61	12.14
La	0.80	0.81	0.88	0.96	–	0.73	0.73	0.83	1.20	2.73	0.71	0.53	1.05	2.14	0.93	0.54	0.89	0.97	0.39
Ce	2.21	2.17	2.29	2.50	–	1.94	2.26	2.29	3.64	7.75	2.28	1.80	3.38	5.98	2.90	1.51	2.48	2.44	1.05
Pr	0.36	0.35	0.35	0.39	–	0.30	0.37	0.37	0.56	1.08	0.38	0.31	0.54	0.86	0.50	0.24	0.40	0.37	0.18
Nd	1.96	1.81	1.83	2.09	–	1.59	1.90	1.86	2.97	5.30	1.94	1.67	2.78	4.18	2.71	1.31	2.09	1.93	0.96
Sm	0.75	0.66	0.66	0.76	–	0.61	0.67	0.67	1.07	1.65	0.72	0.66	1.02	1.37	1.08	0.51	0.77	0.66	0.39
Eu	0.22	0.32	0.21	0.33	–	0.14	0.28	0.32	0.47	0.63	0.23	0.23	0.38	0.48	0.47	0.18	0.27	0.38	0.14
Gd	1.11	1.00	0.95	1.12	–	0.89	1.13	1.18	1.71	2.24	1.22	1.07	1.65	2.10	1.96	0.75	1.12	0.98	0.62
Tb	0.21	0.19	0.18	0.21	–	0.17	0.20	0.21	0.31	0.40	0.22	0.20	0.29	0.36	0.35	0.15	0.22	0.18	0.13
Dy	1.46	1.29	1.20	1.50	–	1.22	1.29	1.36	1.99	2.47	1.43	1.36	1.90	2.30	2.26	1.06	1.56	1.28	0.91
Ho	0.33	0.29	0.27	0.34	–	0.28	0.31	0.31	0.46	0.56	0.32	0.31	0.45	0.51	0.53	0.24	0.36	0.29	0.21
Er	1.00	0.86	0.84	1.02	–	0.86	0.90	0.94	1.34	1.62	0.95	0.92	1.29	1.48	1.54	0.73	1.14	0.87	0.64
Tm	0.15	0.13	0.13	0.15	–	0.13	0.14	0.15	0.20	0.25	0.15	0.15	0.20	0.22	0.23	0.11	0.18	0.13	0.10
Yb	0.99	0.84	0.83	1.01	–	0.86	0.96	1.00	1.40	1.65	1.05	1.03	1.39	1.53	1.56	0.77	1.18	0.88	0.66
Lu	0.16	0.13	0.14	0.16	–	0.14	0.15	0.15	0.22	0.25	0.16	0.16	0.22	0.23	0.24	0.12	0.19	0.14	0.11
Hf	0.58	0.51	0.51	0.58	–	0.51	0.45	0.38	0.63	1.09	0.51	0.49	0.70	0.97	0.73	0.51	0.60	0.57	0.43
Ta	0.10	0.10	0.11	0.09	–	0.06	0.02	0.03	0.05	0.06	0.03	0.02	0.04	0.04	0.02	0.08	0.07	0.08	0.08
Pb	0.56	0.74	0.34	0.48	–	0.58	1.96	3.48	1.38	0.51	0.82	0.66	3.01	1.77	0.53	1.36	1.05	1.38	0.66
Th	0.15	0.14	0.20	0.19	–	0.17	0.15	0.15	0.25	0.52	0.17	0.16	0.19	0.31	0.14	0.14	0.14	0.15	0.11
U	0.10	0.09	0.10	0.10	–	0.10	0.11	0.10	0.19	0.15	0.12	0.09	0.12	0.24	0.10	0.11	0.12	0.10	0.06

4.1. Lower tholeiite unit

Ten of the eleven samples from the lower tholeiite unit plot in the tholeiite field and one plot in the calc-alkaline field due to the effect of crystal fractionation (Fig. 5). FeOt and TiO_2 increase with decreasing MgO (Fig. 6B–D), consistent with low-pressure fractional crystallization of clinopyroxene and plagioclase. The least evolved dyke samples with $Mg^{\#}$ of ~0.60–0.62, has TiO_2 1.10 wt.% and MgO 8.0–8.7 wt.%, Cr 350–400 ppm, and Ni 110–120 ppm and could be parental to the tholeiite samples.

In Chondrite-normalized rare earth element (REE) diagram, samples from the lower tholeiite unit (except for 2SD27) display light REE depletion relative to heavy REEs (Fig. 7A). Chondrite-normalized $[Ce/Sm]_N$ ratio ranges between 0.7 and 1.0 with an average of 0.87, which is slightly higher than that of N-MORB (0.78) (Arévalo and McDonough, 2010). In addition, they have slightly higher REE abundances (22–26×C1) than that of N-MORB (17×C1) despite broad similarity in REE patterns. There is essentially no Eu anomaly. In primitive mantle-normalized multi-element diagrams, they display N-MORB-like patterns with consistent HFSE (Nb, Ta, Zr, Hf and Ti) relative to neighboring elements and varying depletion in Pb and Sr (Fig. 7B). Sample 2SD27 shows broadly an E-MORB-like REE pattern, but has a higher LREE/HREE ratio ($[La/Yb]_N$ 3.3) than that of E-MORB (1.9) (Sun and McDonough, 1989) (Fig. 7A). In terms of major element geochemistry, it is characterized by very high FeOt (15.1 wt.%), TiO_2 (3.1 wt.%) and P_2O_5 (0.5%wt.%), but low MgO (3.8 wt.%), Cr content (5.3 ppm) and Mg# (31), which is consistent with a highly evolved melt derived from a REE enriched parental melt.

4.2. Upper boninite unit

Twenty-eight pillow lava, dyke and gabbro samples from the upper boninitic unit were analyzed and plot in calc-alkaline field (Table 2) (Fig. 5). In MgO variation diagrams (Fig. 6A–C), all the analyzed samples display broadly linear trends with decreasing MgO, suggesting that they are genetically related through fractional crystallization or mixing in a magma chamber. The upper unit samples are characterized by variably high MgO (5.1–22.6 wt.%), Cr (up to 1241 ppm), Ni (to 417 ppm) and SiO_2 (49–61 wt.%) (Table 2, Fig. 6A). The high MgO contents (hence high $Mg^{\#}$ ratios of 0.82–0.57) reflect their very primitive character. Compared to the lower tholeiite samples at a given MgO, the low TiO_2 (0.2–0.5 wt.%) and FeOt (6–10 wt.%) (Table 2, Fig. 6B–C) are also consistent with the boninite melts being derived from a highly refractory harzburgitic source (Falloon and Danyushevsky, 2000).

According to CaO/Al_2O_3 ratios for boninite classification of Crawford et al. (1989), the most primitive boninite glass samples with high MgO (≥15 wt.%) belong to high-Ca boninites (Fig. 6D), similar to high-Ca boninites from North Tonga (Sobolev and Danyushevsky, 1994) and Troodos (Portnyagin et al., 1997; Sobolev et al., 1993), as well as H_2O-bearing harzburgite reaction experimental data (Falloon and Danyushevsky, 2000). Other samples display intermediate characteristics between high-Ca and low-Ca boninite (Fig. 6D), which may be attributed to crystallization of clinopyroxene and particularly late stage of plagioclase fractionation.

On the basis of REE patterns, two types of boninite are identified in the upper boninite unit. The first type of boninites ($n=22$) show light REE depleted patterns with $[La/Sm]_N$ ratios of 0.4–0.9 (Fig. 7A) and relatively low concentrations of REEs and TiO_2, which are termed as low-Ti boninites. The second type of boninites ($n=5$, 4SD03 is from the lower tholeiite unit) are characterized by flat REE patterns and relatively high REE and Ti abundances (Fig. 7A), which are termed as intermediate-Ti boninites. The notably higher concentrations of incompatible elements such as Ti, Zr, Y and rare earth elements, plus flat REE patterns, suggest that intermediate-Ti boninites are unlikely to be the more evolved equivalent of low-Ti type. Instead, they most likely represent a compositionally transitional series between the lower tholeiites and the upper boninites. Sample 4SD03 from the lower tholeiite unit may represent a feeder of the upper (later) boninite melt supply.

Table 3
U, Th and Pb SHRIMP zircon data of two gabbro samples from the DCDB tholeiite–boninite terrane.

Spot	U (ppm)	Th (ppm)	Th/U	$^{206}Pb^*$ (ppm)	$^{206}Pb_C$/(%)	$^{207}Pb^*/^{235}U$	±%	$^{206}Pb^*/^{238}U$	±%	$^{206}Pb/^{238}U$ age(Ma)	±1δ
08QS72-1	321	443	1.42	22.8	−0.06	0.696	2.5	0.083	2.0	511.0	10.0
08QS72-2	138	203	1.52	9.89	0.20	0.660	4.6	0.084	1.7	517.2	8.6
08QS72-3	328	315	0.99	23.5	−0.08	0.691	2.2	0.084	1.6	516.3	7.9
08QS72-4	269	275	1.06	20.3	−0.09	0.717	2.4	0.088	1.6	541.5	8.6
08QS72-5	190	212	1.15	13.7	0.80	0.608	5.2	0.083	1.7	518.5	8.5
08QS72-6	155	183	1.22	11	0.07	0.669	3.7	0.083	1.7	510.9	8.7
08QS72-7	211	274	1.34	15.3	0.24	0.665	2.8	0.084	1.6	519.9	8.2
08QS72-8	238	377	1.64	16.9	0.30	0.656	2.5	0.083	1.6	510.9	8.0
08QS72-9	119	173	1.50	8.57	0.96	0.633	6.3	0.083	1.8	513.6	9.0
08QS72-10	157	160	1.05	11.7	0.29	0.680	3.1	0.086	1.7	534.8	9.1
08QS72-11	98	82	0.86	6.9	0.38	0.668	6.6	0.081	1.9	503.2	9.2
08QS72-12	105	93	0.92	7.83	0.96	0.635	5.4	0.086	1.8	535.6	9.5
08QS72-13	185	191	1.06	13.3	0.38	0.645	3.0	0.083	1.7	515.6	8.4
08QS72-14	159	179	1.16	11.7	0.70	0.614	5.0	0.085	1.7	529.3	8.8
08QS72-15	137	158	1.19	9.43	0.57	0.614	4.1	0.080	1.8	494.5	8.5
08QS72-16	231	350	1.56	17.1	0.44	0.645	6.1	0.086	1.9	532.9	9.7
4SD09-1	52	35	0.70	3.5	3.02	0.541	5.4	0.077	2.7	479.3	14.6
4SD09-2	55	38	0.72	3.9	1.85	0.678	4.4	0.081	2.7	499.5	15.1
4SD09-3	58	37	0.66	4.0	2.86	0.614	4.7	0.076	2.7	475.2	14.1
4SD09-4	182	138	0.79	11.6	0.82	0.602	5.4	0.074	3.5	479.1	18.1
4SD09-5	34	12	0.37	2.5	3.29	0.672	12.7	0.081	2.9	501.8	15.8
4SD09-6	50	38	0.79	3.4	0.81	0.663	4.3	0.079	2.8	491.2	15.2
4SD09-7	42	34	0.84	3.0	3.37	0.704	11.1	0.080	2.9	497.1	17.4
4SD09-8	124	55	0.46	8.0	1.49	0.568	4.1	0.074	2.6	459.8	12.8
4SD09-9	91	79	0.90	6.1	1.31	0.599	3.8	0.077	2.6	480.5	14.3
4SD09-10	35	22	0.66	2.4	3.79	0.612	6.6	0.078	2.9	486.7	16.3
4SD09-11	41	27	0.68	2.8	4.13	0.598	7.3	0.077	4.4	475.8	23.8
4SD09-12	40	29	0.74	2.8	3.22	0.688	7.5	0.079	2.8	492.8	15.8

Pbc and Pb* are common and radiogenic portions, respectively. Common Pb was corrected using measured ^{204}Pb.

5. Zircon U–Pb geochronology

In order to estimate the temporal relationship of DCDB tholeiite–boninite sequence and back-arc-basin development, two gabbroic samples, one (08QS72) from the lower-most part of the tholeiite unit and one (4SD09) from the lower part of the upper boninite unit (see locality in Fig. 2), were chosen for zircon dating. The internal zoning was examined using a cathodoluminescent (CL) spectrometer (Garton Mono CL3+) equipped on a Quanta 200F ESEM with 2-min scanning time at conditions of 15 kV and 120 nA at Peking University. Zircons from the two samples were analyzed for U, Pb and Th isotopes using SHRIMP II at Beijing SHRIMP Centre, Chinese Academy of Geosciences. Instrumental conditions and measurement procedures follow Compston et al. (1992). The spot size of the ion beam was about 25 μm in diameter, and the data were collected in sets of five scans through the masses with 2 nA primary O_2^- beams. The reference zircon was analyzed first and again after every three unknowns. The measured $^{206}Pb/^{238}U$ ratios in the samples were corrected using reference zircon standard SL13 from a pegmatite from Sri Lanka ($^{206}Pb/^{238}U = 0.0928$; 572 Ma) and zircon standard TEMORA (417 Ma) from Australia (Black et al., 2003). The common-Pb correction used the $^{206}Pb/^{204}Pb$ ratio and assumed a two-stage evolution model (Stacey and Kramers, 1975). Analytical results are given in Table 3 and presented on U-Pb Concordia diagrams with 1σ errors in Fig. 8. The mean ages are weighted means at 95% confidence levels.

Zircons from 08QS72 are euhedral and stubby prism with aspect ratios of ~1.5–2.0, and show faint and broad zoning in CL images. The measured Th and U concentrations and Th/U ratio are relatively high (average Th 226 ppm, U 185 ppm and Th/U 1.2). Sixteen analyses yield a concordia weighted mean age of 517 ± 4 Ma (MSWD = 1.6) (Fig. 8A). Zircon grains from sample 4SD09 display low Th (12–138 ppm) and U (34–182 ppm) with Th/U ratios of 0.46–0.90 (Table 3). All the analyzed spots ($n = 12$) are concordant and give a weighted mean age of 487 ± 9 Ma (MSWD = 0.4) (Fig. 8B).

6. Discussion

6.1. Increasing influence of subduction-zone fluids

In order to assess the contribution of slab-derived fluids to the DCDB boninite sequence, we follow the method of Pearce (1983) and Pearce and Peate (1995), which is to draw a baseline through the subduction fluids conservative element Nb, Ta, Zr, Hf, Ti, Y and HREE in MORB-normalized multi-element diagrams. In these diagrams, the area above the baseline represents the subduction contribution of a given element that includes both elements stripped from the slab and elements leached through the mantle wedge by slab-derived fluids. To minimize the crystal fractionation effect, we choose two most primitive glassy samples from every geochemical group. For the lower tholeiites, except for the slight elevation of Rb, Ba and Th, all the analyzed elements coincide well with or slightly lower than the baseline values defined by conservative elements (Fig. 9A–B). On the contrary, both low-Ti and intermediate-Ti boninite display much greater slab contribution, including variable proportions of

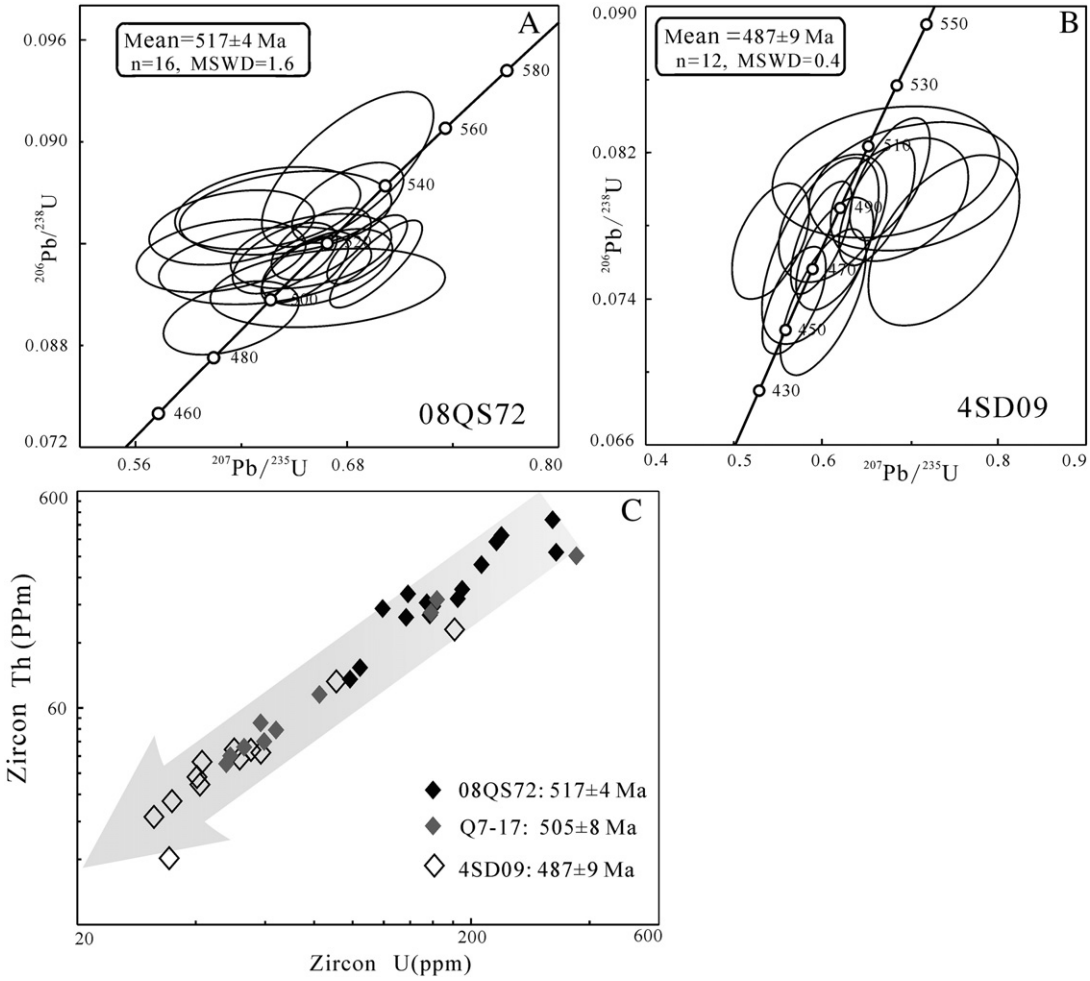

Fig. 8. A–B: Concordia diagrams for two dolerite-gabbro samples (08QS72 and 4SD09) from DCDB tholeiite-boninite terrane (A–B). C: Th–U diagram showing decreasing U and Th contents in zircons from three dated samples with decreasing age. Values for the sample Q7-17 is from Meng et al. (2010).

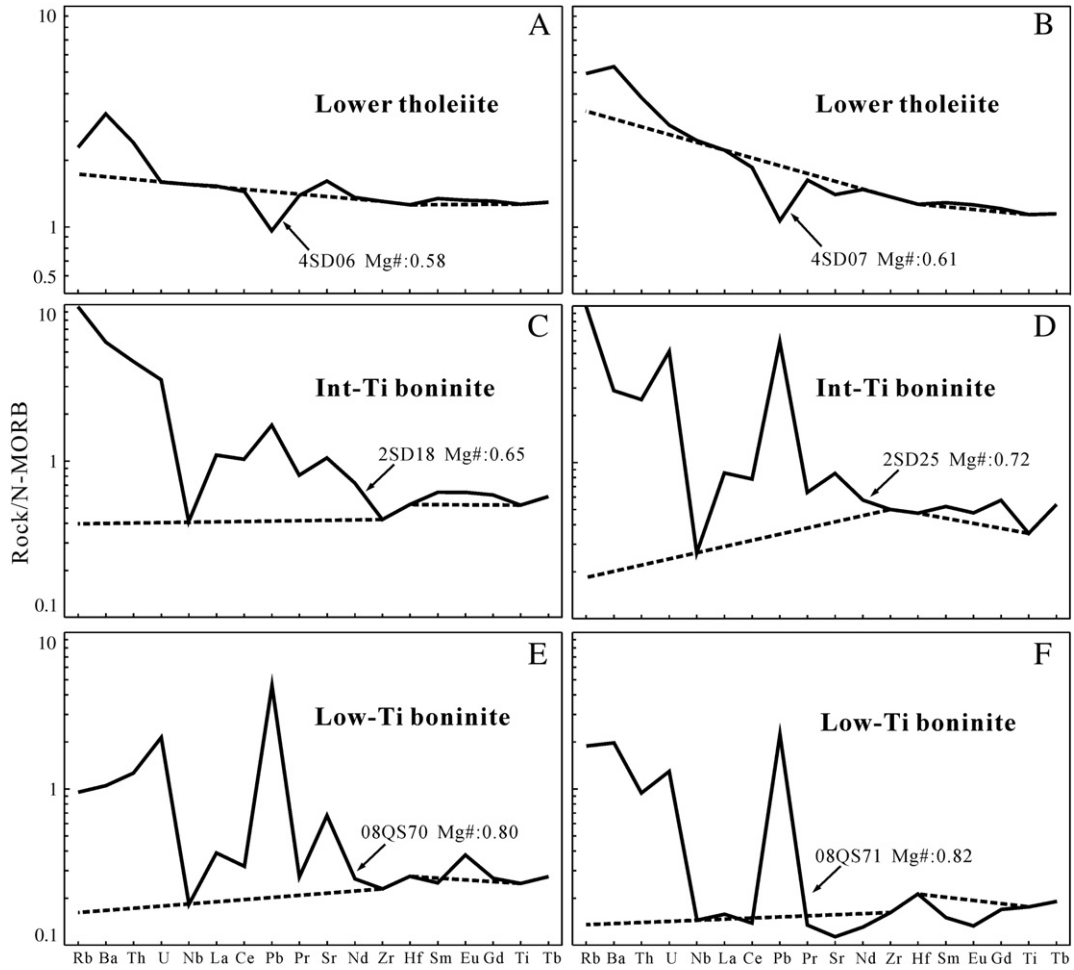

Fig. 9. MORB-normalized trace element diagrams for less fractionated samples of three rock types in the DCDB tholeiite–boninite terrane. A–B: lower tholeiites; C–D: upper intermediate-Ti boninites; E–F: upper low-Ti boninites. Normalizing values and order of elements relative incompatibility during spinel–lherzolite mantle are taken from Sun and McDonough (1989) and Pearce and Parkinson (1993).

LILEs and LREEs (Fig. 9C–F). Further insights to the increasing influence of subduction zone fluids to the petrogenesis of the upper boninites can be investigated using graphs of the M/Yb vs Nb/Yb, where M represents the elements under study, and Nb is widely thought to be least effectively transferred from slab to mantle wedge melting region (Pearce and Peate, 1995; Peate et al., 1997). According to Pearce and Peate (1995), if adding from the slab a variable M to a mantle wedge source of constant composition, the investigated samples will displace from the MORB array to higher M/Yb ratios and form a vertical trend at given Nb/Yb, or plot within a MORB array. Following Pearce et al. (1995), the subduction contribution is quantified by contour lines drawn vertically upward, paralleling to the MORB array (Fig. 10). The local MORB array in this study is defined by oceanic basalts and basaltic samples from the nearby Yushigou ophiolite and Dongcaohe ophiolite, both of which are broadly analogous to mature oceanic fragments (Hou et al., 2006; Tseng et al., 2007). Samples from the lower tholeiites form a linear trend that passes through the average N-MORB to average E-MORB composition, suggesting that mantle contributes nearly 100% of Nd, Zr, Th, and La through the peridotite melting process. On the contrary, both low-Ti and intermediate-Ti boninite are markedly displaced upwards from the MORB array to high Th/Yb and La/Yb ratios (Fig. 10 A–B). The subduction contributions of Th for both types of boninites range from ~70 up to 85% (Fig. 10A), and intermediate-Ti boninites displays slightly higher subduction contribution in La (20–60%) than that of low-Ti boninite (0–30%) (Fig. 10B). In the Nd/Yb and Zr/Yb vs. Nb/Yb diagram (Fig. 10C–D), nearly all boninite samples are plotted within the MORB array, from the average N-MORB to progressively depleted trend, supporting a mantle wedge origin for almost all Nd and Zr.

The Th and U systematics (Th, U concentrations and Th/U ratios) can also be independently used for identifying and tracing source characteristics and petrogenetic processes. Despite variable U and Th contents, samples from the lower tholeiite unit collectively form a linear trend between reference lines defined by N-MORB (0.39) and Primitive mantle (0.25) (Fig. 11A). Therefore, the uniform and mantle-like Th/U ratios further provide concrete evidence that addition of U and Th from subducting slab is insignificant during the petrogenesis of the lower tholeiite unit. Most low-Ti boninite samples display intermediate and uniform contents of U (0.09–0.13 ppm) and Th (0.11–0.20 ppm) except for two samples (Fig. 11A). However, the extremely depleted character demonstrated by major, trace and mineral geochemistry does not support the existence of high U and Th abundances in boninite source. Thus, the markedly elevated Th (1.7–0.9 × N-MORB) and U (2.7–1.9 × N-MORB) is best interpreted to be introduced from slab-derived fluids. Compared to low-Ti boninite, the intermediate-Ti boninites have relatively high and variable Th and U contents. Three of five samples are displaced to high U and U/Th ratios and other two exhibit lower-tholeiite-like U/Th ratios. This reflects significant compositional variations of slab-derived fluids and/or non-uniform metasomatism of mantle wedge at least at the time of intermediate-Ti boninite generation. Consequently, the intermediate-Ti boninites appear to represent a transitional situation between boninite and low-Ti boninite in terms of increasing influence of subduction-zone fluids.

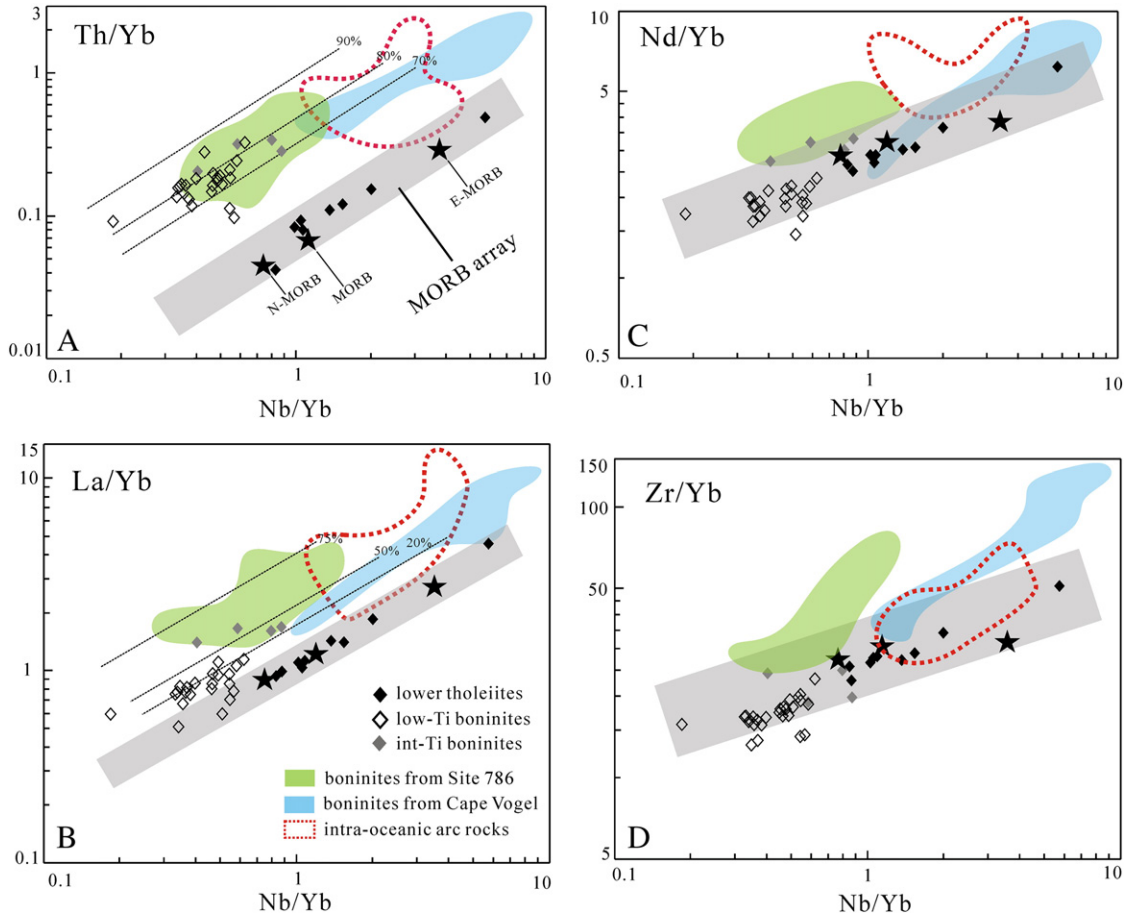

Fig. 10. Trace element ratio plots of (A) Th/Yb, (B) La/Yb, (C) Nd/Yb and (D) Zr/Yb vs. Nb/Yb for the DCDB boninites. The area of the shaded rectangle shows the local MORB-array defined by oceanic basalts and local basaltic rocks (see the text). The fields for typical for-arc boninites from Cape Vogel and Site 786 and arc rocks worldwide are shown for comparison (references see the text). The thin broken lines represent contours of % subduction zone contribution for a given element in the mantle (Pearce et al., 1995). Average N-MORB and MORB values are from Arévalo and McDonough (2010). E-MORB value is from Sun and McDonough (1989).

6.2. Mantle source P-T modeling and partial melting

Geochemically, the MORB-like lower tholeiites are considered to be generated by decompression-dominated partial melting of a depleted MORB Mantle (DMM) source without (or with little) influence of slab-derived components. Therefore, a simple aggregated fractional melting modeling is developed in order to quantify the extent of melting. The source mantle compositions and bulk partition coefficients (*D*) used in our model are taken from Workman and Hart (2005). Following the method of Niu and Collerson (1999); Niu et al. (2002); Niu and O'Hara, (2008), the parent magma for lower tholeiites can be obtained by extrapolating the compositions of the least fractionated samples along liquid lines of descent back to equilibrium with melt composition with $Mg^{\#} = 72$ and of crystallized olivine of $F_{O89.6}$. Compared to the least fractionated sample (4SD07, Mg#: 0.61; MgO: 8 wt.%), the obtained parent magma for lower tholeiites (labeled as "P" in Fig. 12) has slightly lower absolute abundances for nearly all trace elements. As shown in Fig. 12, the least evolved sample (4SD07) can be best simulated by 5% melting of enriched DMM, where most incompatible elements show an excellent fit except for a small discrepancy in Rb, Ba, Th, U and Sr. For fractionation-corrected parent magma, slightly greater degree of about 6% melting is required (Fig. 12). The 5–6% melting of enriched DMM to generate lower tholeiites is generally close to recent estimates of ~6% melting to produce global average MORB (Workman and Hart, 2005) although the average extent of melting beneath global ocean ridges remain debatable (see Salters and Stracke, 2004; Niu and O'Hara, 2009).

Given depleted major and trace element and mineral geochemistry for boninites, the depleted DMM from Workman and Hart (2005) is here used as a model mantle source for DCDB boninites. As shown in Fig. 12, about 15% melting of depleted DMM produces a good fit to the glass sample 08QS70 except for a large discrepancy in Rb, Ba, Th, U, Pb and Sr due to input from slab-derived components. To produce another least evolved glass sample (08QS71) of low-Ti boninites, at least 25% melting of the depleted DMM is required. In fact, large discrepancy in REE and HFSE patterns and absolute concentrations between the modeling results and observed values suggest that the depleted DMM is clearly not viable for the pre-melting source of partial DCDB boninite samples and a good correspondence may be achieved if assuming a much greater extent of melt extraction by previous melting events. Numerous studies show that boninite generation needs re-melting of previously melt-extracted mantle source i.e. at least two-stage melting process (e.g., Duncan and Green, 1987; Crawford et al., 1989; Bédard, 1999; Pagé et al., 2009). According to most recent modeling results by Pagé (2009), the Thetford Mines boninites represent the products of an additional 10–20% melting of extremely refractory mantle, which have previously undergone 15–20% melting. And the Betts Cove low-Ti boninites were extracted from a mantle source residual after previous 20–22% melting of fertile mantle. In fact, it is difficult to precisely evaluate the degree of melting for the DCDB boninite generation because of many uncertainties such as the mineralogy-dependent bulk D values, pre-melting source compositions and the effect of the aforementioned slab components (e.g., Bédard, 1999; Pagé et al., 2009). However, a series of plots

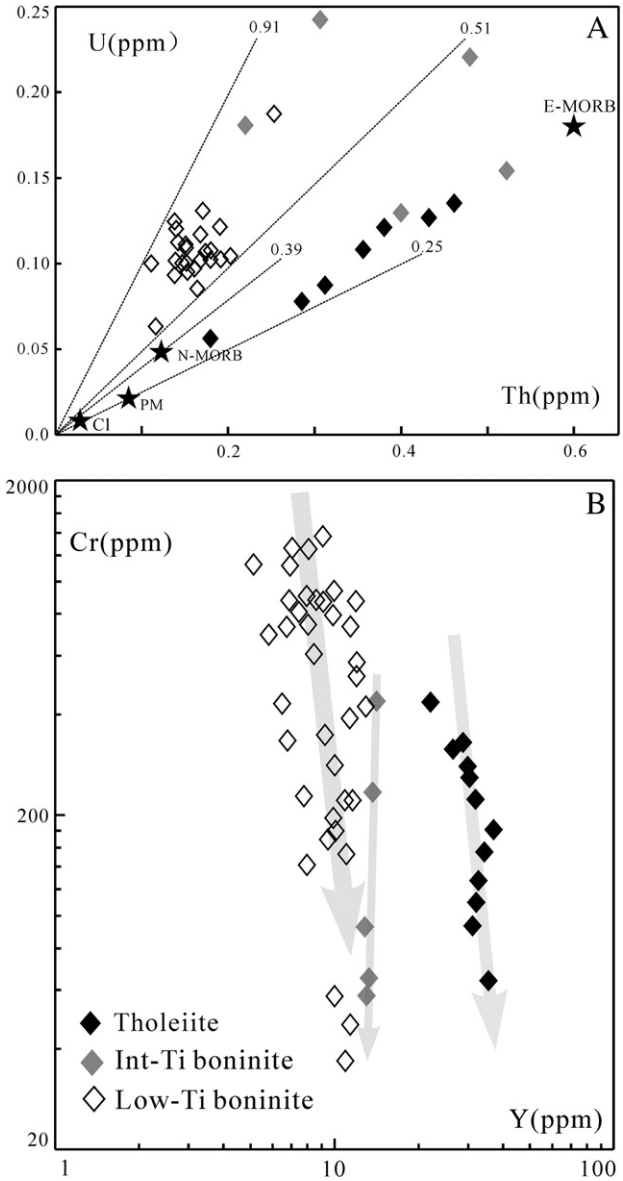

Fig. 11. Plots of (A) Th/ U and (B) Cr/Y for three main geochemical groups of the DCDB tholeiite–boninite rocks showing varied and increasing subduction zone fluids influence and degree of melting. PM, E-MORB and OIB values are from Sun and McDonough (1989). Average N-MORB value is from Arévalo Jr. and McDonough (2010).

(Figs. 9, 10, 11A), including the Cr-Y diagram (Fig. 11B), together with extremely refractory major (Fig. 6B–C) and trace element (Fig. 7) and mineral geochemistry (Fig. 4) call for an obvious increase of degree of melting and/or source depletion for DCDB upper boninite generation. Note that, as shown in Fig. 8C, U, Th contents and Th/U ratios of zircons in the three dated samples, from lower to upper position of DCDB tholeiite–boninite sequence, exhibit a systematic decrease with ages from 517 Ma, 505 Ma to 487 Ma. This observation again argues that the mantle sources do become increasingly more refractory from the lower to upper unit of the terrane with time.

Experimental data have shown a liner correlation between MgO contents of primary basaltic liquids and mantle potential temperature at a given pressure (e.g., Tatsumi, 1981, 1982; Umino and Kushiro, 1989; Sugawara, 2000). All spinel phenocrysts or inclusions from DCDB boninitic samples have very uniform Cr# of 0.78 to 0.81, that is, liquidus spinel Cr# remains nearly constant despite the coexisting melt may not be primary. Based on the Fo-Cr# mantle array by Arai (1987, 1990), the olivine in equilibrium with such spinel Cr# should have Fo values in the range of 91.6 to 93.8. The coexisting primary melt accordingly has $Mg^{\#}$ values in the range of 78 to 82, if assuming the olivine–melt K_D ($K_D = [FeO/MgO]^{liq}/[FeO/MgO]^{olive}$) between 0.3 and 0.33. Based on the linear relationship between MgO and $Mg^{\#}$, we conclude that only glass samples with MgO > 15 wt.% may represent the primary boninitic compositions. Furthermore, the primary melt composition also require Al_2O_3 and TiO_2 in the range of 8.8–11.9 wt.% and 0.19–0.4 wt.%, respectively, which is independently constrained by Sp-melt composition relationship after the method of Kamenetsky et al. (2001). Consequently, only 7 glass samples have compositions satisfying these criterions and most likely represent the primary (or close to) compositions for the DCDB upper boninite magma.

Given the fact that hydrous fluids/melts are obviously involved, the P–T conditions of primary DCDB high-Ca boninite are best determined by using the petrogenetic grid for H_2O-undersaturated melting of depleted mantle by Falloon and Danyushevsky (2000). As seen in Fig. 13, the DCDB high-Ca boninites plot in a scattered range from 1.4 GPa to 2.2 GPa, which is generally higher than 1.5 GPa for Troodos and North Tonga high-Ca boninite calculated by using the same technique. More restricted pressure range may be achieved if more precise primary compositions for the DCDB boninite can be determined. There is, however, the possibility that continuous melting itself most likely occurred over a wide region and depth within the melting region. Based on the linear relationship between MgO and T determined by harzburgite reaction experiment at 2.0 GPa (Fallon and Danyushevsky, 2000), the liquid temperatures are in the range of 1380–1460 °C and 1470–1547 °C under wet and dry conditions, respectively. Given the obvious subduction fluid signatures, the former is realistic for the case of DCDB boninite generation. The mantle potential temperature of 1380–1460 °C is similar to that of North Tonga and Troodos high-Ca boninite obtained by melt inclusions study (e.g., Sobolev et al., 1993; Sobolev and Danyushevsky, 1994). Mantle potential P-T conditions for the lower tholeiites are assumed to be the same as MORB beneath the mid-ocean ridge (Tp = 1315 °C, McKenzie et al., 2005; Asimov et al., 1995; Tp = 1297 °C–1377 °C, Niu and O'Hara, 2008) due to its similarity to MORB in composition and degree of melting. This means that there is a marked mantle potential temperate increase of at least 100 °C from the condition of DCDB tholeiites to boninites.

To account for the high temperature for North-Tonga high-Ca boninite, Danyushevsky et al. (1995) invoked intrusion of Samoa mantle plume at the termination of the Tonga trench. This model reasonably explains the North-Tonga boninite composition such as wide range of REE contents (from strongly depleted to strongly enriched) and similarity in Sr, Nd and Pb isotopic values with OIB-type lavas from the Samoa mantle plume (e.g., Danyushevsky et al., 1995; Falloon et al., 2007). However, there is little petrochemical evidence to support plume-related source mantle involved in DCDB boninite petrogenesis. In fact, very few cases were demonstrated to display any involvement of OIB-like enriched component in the genesis for boninite suites worldwide. Recently, to account for the excess heat source for boninite generation, lithospheric extension and hot asthenospheric upwelling have been increasingly stressed and embedded into tectonic and petrogenic models for boninites (e.g., Kurth-velz et al., 1998; Bédard, 1999; Kurth-velz et al., 2004).Three general tectonic scenarios have been proposed: 1) upwelling of asthenosphere during subduction initiation based on IBM fore-arc boninitic volcanism (e.g., Ishizuka et al., 2006, 2) upwelling of MORB mantle diapirs caused by new back-arc propagation or spreading such as in the central Lau basin (e.g., Falloon et al., 1992) and Eastern Manus basin (e.g., Niedermeier et al., 2008), and 3) convection and upwelling of asthenosphere at slab edges similar to what has been suggested for the Troodos (e.g., Pearce and Robinson, 2010) and Hunter Ridge (e.g., Monzier et al., 1993). These tectonic settings are exclusively related to fast slab/trench rollback and intensive extension-dominated tectonic regime, which has

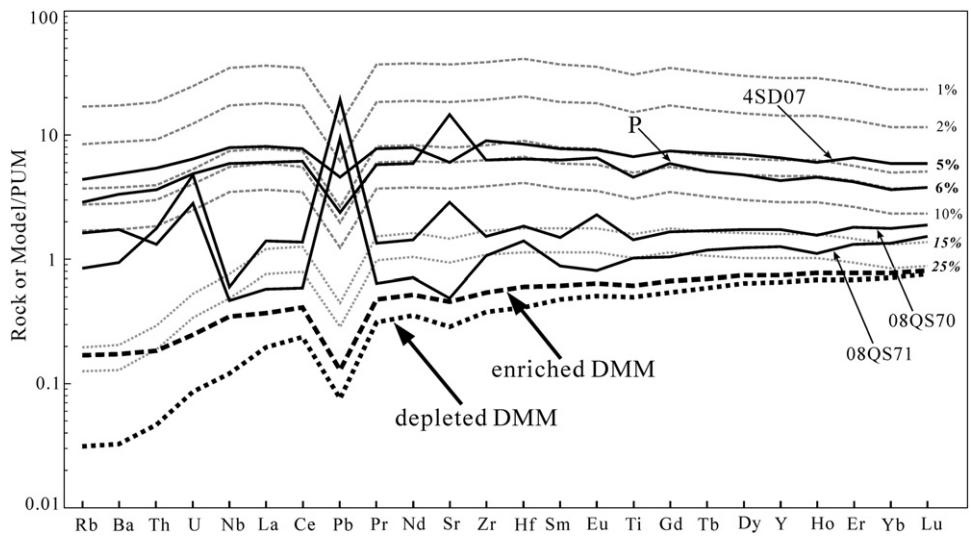

Fig. 12. Liquids produced by aggregated fractional melting of the enriched and depleted DMM source from Workman and Hart (2005) (detailed discussion see the text).

allowed hot and hydrous mantle to upwell adiabatically. To precisely identify the specific tectonic environment and geodynamic processes for the Paleozoic DCDB boninite generation is not straightforward. According to geochemical and geochronological data, a likely scenario for a marked mantle potential temperate increase from DCDB tholeiite to boninite is related to upwelling of asthenosphere during the earliest stage of continuing rupture and rifting of back-arc lithosphere.

6.3. Comparison with other boninite association worldwide

6.3.1. The absence of LREE and Zr–Hf enrichment

The majority of worldwide boninite suites display variable light REE (or LREE) -enrichment with two subtypes: E-type (strong LREE enrichment) and C-type (well known as U-shaped). Bulk and mineral geochemistry suggest that boninite sources are extremely refractory, thus this discordant LREE enrichment is commonly ascribed to second-stage re-enrichment process before or during boninite generation. However, the LREE-depleted patterns for the DCDB boninites (Fig. 7A) obviously differ from the majority of worldwide boninite suites, suggesting significant difference in slab-derived fluids/melts. Fig. 14 compares Ti/Zr ratios of DCDB boninite with other boninites previously reported. The great majority of boninites display marked variations in Zr contents within a restricted range of TiO_2 contents, resulting in a highly variable and notably depressed Ti/Zr ratio. In particular, boninites from Marianna trench (Bloomer and Hawkins, 1987) and Nepoui, New Caledonia (Cameron, 1989) show a sub-horizontal linear trend in the plot of TiO_2 Vs Zr (Fig. 14), reflecting the pronounced Zr re-enrichment. On the contrary, the DCDB boninites display high Ti/Zr ratios between 96 and 136 (average 112.5), similar to boninites from Oman, Troodos and North Tonga and resembling primitive mantle (PM) (116) and N-MORB (99) (Arévalo Jr. and McDonough 2010). Experimental data and studies on natural samples suggest that Ti and Zr are not significantly fractionated during basaltic melt generation because of their very sufficiently similar K_D during peridotite melting. Therefore, the primitive mantle- and N-MORB-like Ti/Zr ratios of DCDB boninites are most likely inherited from their former depleted mantle source, reflecting no slab-derived metasomatic modification on Zr and Ti. In Fig. 10A, DCDB boninites display equivalent enrichment in Th with arc basalts and fore-arc-related low-Ca boninites. In the La/Yb and Nd/Yb vs. Nb/Yb diagrams (Fig. 10B–C), DCDB boninites display much less mobility in LREE (La and Nd) compared to the formers. The significant enrichment of Th suggests that slab components invading into DCDB boninite source is not likely simple aqueous fluids. However, we must emphasize that contribution of hydrous melt to DCDB boninites genesis is much less than to fore-arc low-Ca boninites and arc basalts. Thus, the enriching components are compositionally water-rich and Zr–Hf-free, in which water-soluble elements (mainly including Cs, Rb, Ba, Pb, Sr, Th and U) are the main solutes and significant and minor amounts of Th and LREE (mainly La) are involved. The trace element spectra of such 'limpid' hydrous fluids/melts share many similarities with that observed in typical back arc basin basalts (BABB) away from the volcanic front (e.g., Falloon et al., 1992; Taylor and Martinez, 2003).

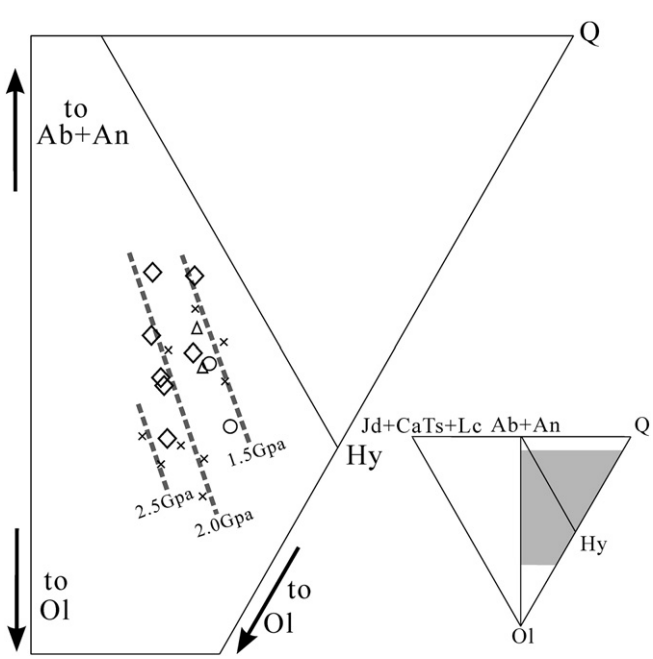

Fig. 13. Comparison of the primary DCDB boninite compositions (open diamonds) with boninites Tonga (open triangles), Troodos (circles) and the experimentally determined refractory peridotite melting cotectics in the molecular normative projection from Ol onto the face Jd + CaTs + Lc-Di-Q of the 'basalt tetrahedron'. The crosses and thin dashed lines are Ol + OPX + L cotectics under H2O-undersaturated conditions at 1.5, 2.0 and 2.5 Gpa, respectively, determined by the boninite–harzburgite reaction experiments of Falloon and Danyushevsky (2000).

6.3.2. Interpretation and tectonic implications

In Fig. 16A, we have compiled REE and Zr–Hf data available from 17 reported boninite localities. When examining single localities,

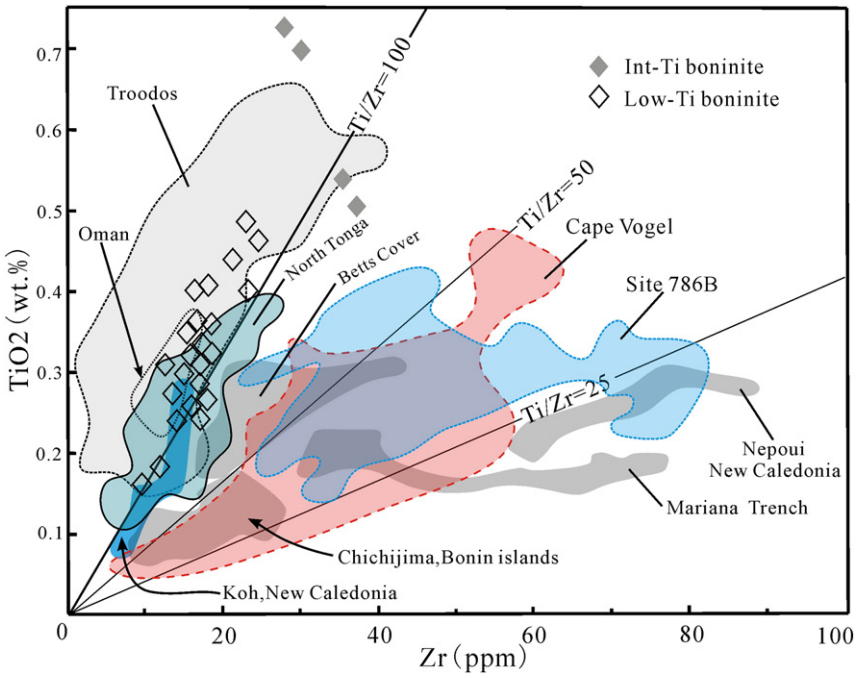

Fig. 14. TiO2 vs. Zr diagram for comparing Ti/Zr ratio values of the DCDB boninites with boninites worldwide. Source of the data: Chichijima, Bonin Islands, Hickey and Frey (1982) and Taylor et al. (1994); Cape Vogel, Jenner (1981), Hickey and Frey (1982) and König et al. (2010); Site 786B, Pearce et al. (1992) and Murton et al. (1992); Mariana Trench, Hickey and Frey (1982) and Bloomer and Hawkins (1987); Nepoui, New Caledonia, Sameshima et al. (1983) and Cameron (1989); Betts Cover, Bédard (1999); Koh, New Caledonia, Cameron (1989) and Meffre et al.(1996); Troodos, Cameron (1985) and Flower and Levine (1987); North Tonga, Falloon and Crawford (1991), Sobolev and Danyushevsky (1994), Wendt et al. (1997) and Falloon et al. (2007, 2008); Oman ophiolite, Ishikawa et al., 2002.

most boninite suites such as Chichijima, Bonin Islands, Mariana Trench, Cape Vogel from New Caledonia, Betts cover, Pindos and Troodos, display a broadly positive correlation between La/Sm and Zr/Sm. And such a linear relationship suffers from only a few exceptions, like DSDP site 458, Guam and Koh from New Caledonia, probably due to limited sampling. If we extend individual locality to the global analysis, a statistically significant positive trend is apparent. This observation provides convincing evidence for a first-order intrinsic link between LREE and Zr–Hf enrichment in boninitic rocks (both are in the numerator with a common denominator Sm). In other words, both LREEs (such as La) and Zr–Hf share the common source and are controlled by the same mechanism. Moreover, the Zr–La array for boninite worldwide (the dotted lines in Fig. 15A) clearly deviates from the field of primitive arc basalts (values from Kelemen et al., 2003), suggesting the variable involvement of a slab-derived hydrous melt in boninite genesis. In Fig. 15A, the samples from DCDB boninite with overlapping fields of Troodos are plotted in the left-down end of boninite Zr–La array, which reflects trace involvement of slab-derived melt in its genesis, as discussed previously.

In the Izu-Bonin-Mariana arc-basin system, large volumes of boninitic melts generated simultaneously at ca. 48–45 Ma (e.g., Ishizuka et al., 2006) are exposed from Mariana trench to fore-arc region (Bonin ridge, ODP site 786 and 458) to separated remnant arc including islands of Guam, Saipan and Palau (Kobayashi, 2004). In Ti/Zr vs. Zr/Sm diagram (Fig. 15B), these boninite suites show a systematic decrease in slab-derived signatures with increasing distance from trench within single arc system. In Fig. 15B, DCDB boninites plot in the overlapping fields of boninites from the North Tonga and Troodos ophiolite with back-arc basin origin (e.g., Moores et al., 1984; Flower and Levine, 1987), contrasting with the field for fore-arc extension-related boninites represented by those from IBM subduction system and Cape Vogel boninites (Jaques and Chappell, 1980; König et al., 2010). The first-order decrease of Zr/Sm enrichment with increasing distance from trench (Fig. 15B) suggests that in addition to varying melts/fluids compositions and heterogeneous metasomatism in the mantle wedge, the distance from boninite sources to subducted slab (or trench) should act as a main function of the LREE-Zr–Hf enrichment array observed in Fig. 15A and B. Compared to fore-arc boninites, back-arc basin-related boninites are characterized by the involvement of a larger proportion of sub-back-arc mantle materials, but much less in terms of slab-derived components due to further distance to trench (or slab). For this reason, back-arc basin-related boninites generally display MORB-like or more depleted (i.e. higher) Ti/Zr values that are largely inherited from mantle source. Together with boninite chemical signatures (e.g., high-Ca or low-Ca type) and rock association (BABB/N-MORB or arc volcanic series), the degree of LREE-Zr–Hf enrichment is thus expected to be a useful indicator for specific tectonic settings for ancient boninite terranes.

6.4. Implications of DCDB tholeiite–boninite terrane

Systematic studies on boninitic terranes from the IBM subduction system have led to the prevalent view on the petrogenesis of boninite and boninite-like rocks, i.e., the subduction initiation model (e.g., Stern and Bloomer, 1992; Hall et al., 2003; Niu et al., 2003; Stern, 2004). According to this model, when old lithosphere begins to subside, the asthenosphere upwells towards the fore-arc region directly above the top of the shallow dipping slab, and undergoes decompression melting and brief fore-arc spreading (Stern and Bloomer, 1992; Hall et al., 2003; Stern, 2004). As the old lithosphere continues to subside, the asthenosphere upwelling center at depth and extension-induced melting locus is inclined to migrate away from trench toward back-arc regions, since the mantle wedge beneath the fore-arc becomes increasingly cold and cannot sustain large-scale mantle flow. Meanwhile, increasingly deepened slab acts as a greater barrier for mantle flow into fore-arc regions orthogonal to trench (Pearce and Robinson, 2010). The geochemical and geochronological data documented in this paper support that DCDB tholeiite–boninite association records such an important migration of upwelling asthenosphere from the initiation of subduction to the development of back-arc basin.

The DCDB tholeiite–boninite terrane shows a magmatic progression from MORB-like tholeiites produced in a relatively “dry” and fertile

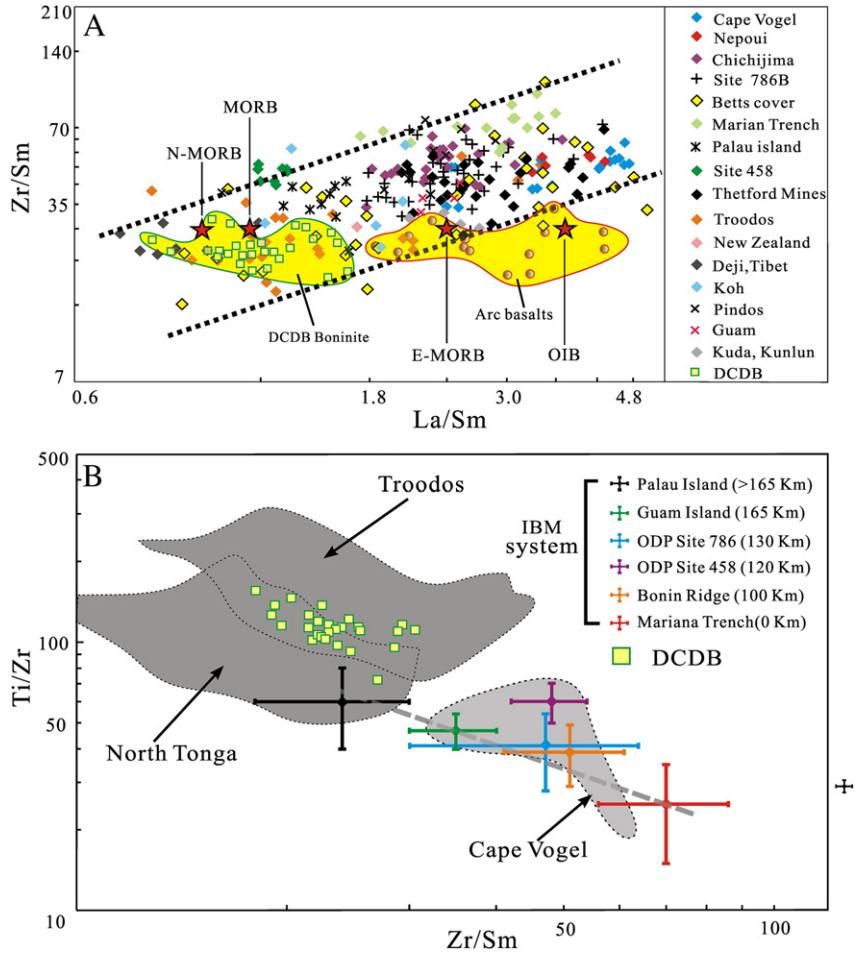

Fig. 15. A: Zr/Sm vs. La/Sm for 17 boninites localities worldwide. Two thick dashed lines show a good positive statistical correlation between La/Sm and Zr/Sm. Data sources: Palau Island, Hawkins and Castillo (1998); Site 458, Sharaskin (1981) and Hickey and Frey (1981); Thetford Mines, Pagé et al. (2009); New Zealand, Wood (1980); Deji, Tibet, Chen et al. (2003); Pindos Pe-Piper et al. (2004); Guam, Hickey-Vargas and Reagan (1987), Kuda, Kunlun , Yuan et al. (2002). All data for other boninite series see Fig. 14. The field for typical intra oceanic-arc rocks is shown for comparison (Kelemen et al., 2003). Average N-MORB and MORB values are from Arévalo and McDonough (2010). E-MORB value is from Sun and McDonough (1989). B: Ti/Zr vs. Zr/Sm diagram for back-arc basin-origin high-Ca boninite (North Tonga and Troodos ophilite) and fore-arc extension-related low-Ca boninites from IBM and Cape Vogel.

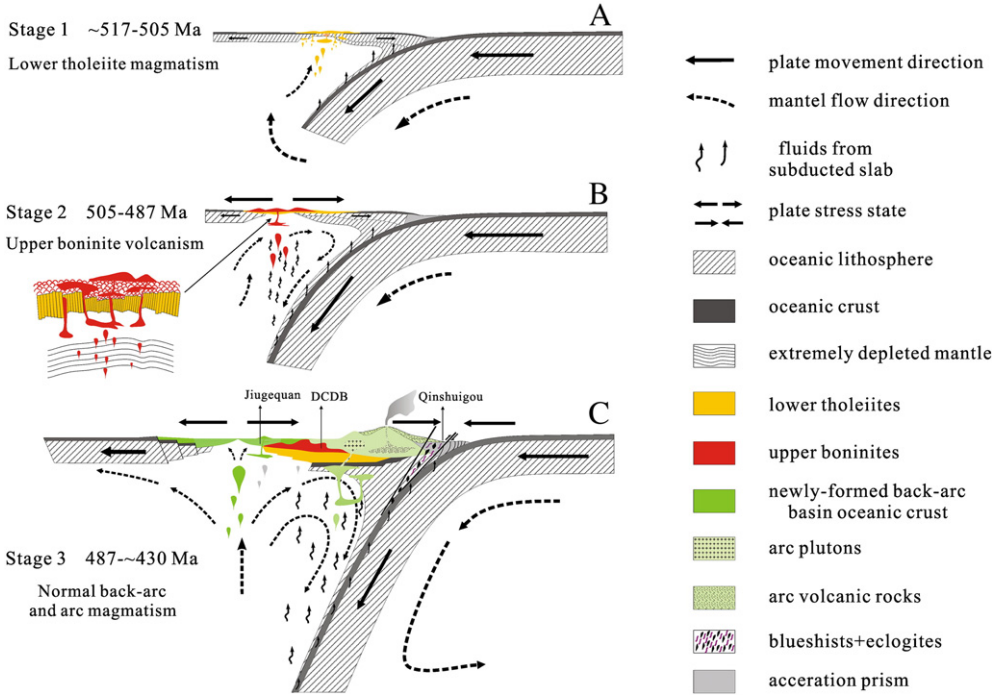

Fig. 16. Schematic model for tectono-magmatic evolution and genesis of the DCDB tholeiite–boninite terrane.

mantle to extremely depleted low-Ti boninites with strong influence of slab-derived fluids/melts. The mineral and bulk-rock geochemistry of the upper boninites show strong similarities to back-arc basin-related boninites such as those from CLSC and ELSC of Lau basin (e.g., Falloon et al., 1992), North Tonga (e.g., Sobolev and Danyushevsky, 1994), Hunter Ridge (e.g., Monzier et al., 1993) and Eastern Manus (Niedermeier et al., 2008; Rubin et al., 2009). Therefore, the lower tholeiite unit with ages of 517–505 Ma represents the earliest infant arc magma by decompression-induced partial melting of the upwelling asthenospheric mantle in response to the onset of subduction initiation (Fig. 16A). The upper boninite unit with younger age of 487 ± 9 Ma is interpreted as earliest products of infant arc splitting (Fig. 16B) and subsequent back-arc basin development (Fig. 16C). The elevated mantle potential temperature of 1380–1460 °C for generating the upper boninite unit reflects a higher proportion of hot asthenosphere rose into the melting region. Large volumes of subduction-zone fluids/melts released from the front of subducting slab at greater depth migrate upward by virtue of upwelling mantle diapirs at the beginning of back-arc extension (Fig. 16B). With the aid of a combination of extra heat from the adiabatically-upwelled asthenosphere, slab-derived hydrous fluids/melts and extension of over-riding upper plate, re-melting of the depleted, serpentinized mantle resulted in the eventual eruption of upper boninites. Large compositional variation of the upper boninite unit reflect complex and long-term melt extraction and differentiation, heterogeneous mantle source and variable degree of mantle metasomatism by slab-derived hydrous fluids/melts.

Acknowledgments

We thank L. Su for helping with whole-rock analyses, H.Q. Xie and D.Y. Liu for SHRIMP dating and G.M. Shu for EPMA analyses. We also thank the two anonymous reviewers and the guest editor Y.F. Zheng for their detailed and constructive comments, which led to a better presentation of the final product. This study was supported by the Major State Basic Research Development Projects (2009CB825007), National Natural Science Foundation of China (Grant Nos. 40825007, 40821002, 40773012, 91014003) and Basic geological survey program of China Geological Survey (1212010911070).

References

Arai, S., 1987. An estimation of the least depleted spinel peridotite on the basis of olivine-spinel mantle array. Neues Jahrbuch für Mineralogie Monatsheft 8, 347–354.
Arai, S., 1990. What kind of magma could be equilibrated with ophiolitic peridotites? In: Malpas, J., Moores, E.M., Panayiotou, A., Xenophontos, C. (Eds.), Ophiolites. Cyprus Geological Survey, Nicosia, Cyprus, pp. 557–584.
Arculus, R.J., Pearce, J.A., Murton, B.J., Van der Laan, S.R., 1992. Igneous stratigraphy and major element geochemistry of Holes 786A and 786B. In: Fryer, P., Pearce, J.A., Stokking, L.B. (Eds.), Proc. ODP, Sci. Results, 125, pp. 143–169.
Arévalo Jr., R., McDonough, W.F., 2010. Chemical variations and regional diversity observed in MORB. Chemical Geology 271, 70–85.
Ariskin, A.A., Nikolaev, G.S., 1996. An empirical model for the calculation of spinel-melt equilibrium in mafic igneous systems at atmospheric pressure: 1. Chromian spinels. Contributions to Mineralogy and Petrology 123, 282–292.
Asimov, P.D., Hirschmann, M.M., Ghiorso, M.S., O'Hara, M.J., Stolper, E.M., 1995. The effect of pressure-induced solid–solid phase transitions on decompression melting of the mantle. Geochimica et Cosmochimica Acta 59, 4489–4506.
Barnes, S.J., Roeder, P., 2001. The range of spinel compositions in terrestrial mafic and ultramafic rocks. Journal of Petrology 42, 2279–2302.
Bédard, J.H., 1999. Petrogenesis of boninites from the Betts Cove ophiolite, Newfoundland, Canada: identification of subducted source components. Journal of Petrology 40, 1853–1889.
Bédard, J.H., Lauziere, K., Tremblay, A., Sangster, A., 1998. Evidence for forearc seafloor-spreading from the Betts Cove ophiolite, Newfoundland: oceanic crust of boninitic affinity. Tectonophysics 284, 233–245.
Bednarz, Z., Schmincke, H., 1994. Petrological and chemical evolution of the Northeastern Troodos extrusive series, Cyprus. Journal of Petrology 35, 489–523.
Black, L.P., Kamo, S.L., Allen, C.M., Aleinikoff, J.N., Davis, D.W., Korsch, R.J., Foudoulis, C., 2003. TEMORA 1: a new zircon standard for Phanerozoic U–Pb geochronology. Chemical Geology 200, 155–170.
Bloomer, S.H., Hawkins, J.W., 1987. Petrology and geochemistry of boninites series volcanic rocks from the Mariana trench. Contributions to Mineralogy and Petrology 97, 361–377.
Bloomer, S.H., Taylor, B., MacLeod, C.J., Stern, R.J., Fryer, P., Hawkins, J.W., Johnson, L., 1995. Early arc volcanism and the ophiolite problem: a perspective from drilling in the Western Pacific. In: Taylor, B., Natland, J. (Eds.), Active Margins and Marginal Basins of the Western Pacific: AGU Geophys. Monogr., 88, pp. 1–30.
Boespflug, X., Dosso, L., Bougault, H., Joron, J.L., 1990. Trace element and isotopic (Sr and Nd) geochemistry of volcanic rocks from the Lau Basin. In: von Stackelberg, U., von Rad, U. (Eds.), Geological Evolution and Hydrothermal Activity in the Lau and North Fiji Basins, South-west Pacific Ocean (Results of SONNE Cruise SO-35): Geol. Jahrb.,Reihe D, 92, pp. 503–516.
Cameron, W.E., 1985. Petrology and origin of primitive lavas from the Troodos ophiolite, Cyprus. Contributions to Mineralogy and Petrology 89, 256–262.
Cameron, W.E., 1989. Contrasting boninite–tholeiite associations from New Caledonia. In: Chen, Y., Zhou, D.J., Wang, E., Li, X.Y. (Eds.), Geochemical Characteristics of Boninite Series Rocks Found in Dachadaban Ophiolite Sunan Country, North Qilian Mountain: Acta Petrolei Sinica, 11, pp. 147–153 (Suppl).
Chen, Y., Zhou, D.J., Wang, E.C., Li, X.Y., 1995. Geochemical characteristics of boninite series rocks found in Dachadaban ophiolite, Sunan County, North Qilian Mountains. Acta Petrologica Mineralogica 11, 145–153.
Chen, G.W., Xia, B., Zhong, Z.H., Wang, G.Q., Wang, H., Zhao, T.P., Wang, J.C., Zhang, L., Qi, L., Li, S.R., 2003. Geochemical characteristics and geological significance of boninites in the Deji ophiolite, Tibet. Acta Mineralogica Sinica 23, 91–96.
Compston, W., Williams, I.S., Kirschvink, J.L., Zhang, Z., Ma, G., 1992. Zircon U–Pb ages for the Early Cambrian time-scale. Journal of the Geological Society 149, 171–184.
Crawford, A.J., Keays, R.R., 1987. Petrogenesis of Victorian Cambrian tholeiites and implications for the origin of associated boninites. Journal of Petrology 28, 1075–1109.
Crawford, A.J., Beccaluva, L., Serri, G., 1981. Tectono-magmatic evolution of the West Philippine-Mariana region and the origin of boninites. Earth and Planetary Science Letters 54, 346–356.
Crawford, A.J., Falloon, T.J., Green, D.H., 1989. Classification, petrogenesis and tectonic setting of boninites. In: Crawford, A.J. (Ed.), Boninites and Related Rocks. Unwin Hyman, London, pp. 1–49.
Danyushevsky, L.V., Sobolev, A.V., Falloon, T.J., 1995. North Tonga high-Ca boninite petrogenesis: the role of Samoan plume and subduction zone-transform fault transition. Journal of Geodynamics 20, 219–241.
Dick, H.J.B., Bullen, T., 1984. Chromian spinel as a petrogenetic indicator in abyssal and alpine-type peridotites and spatially associated lavas. Contributions to Mineralogy and Petrology 86, 54–76.
Dilek, Y., Thy, P., 2009. Island arc tholeiite to boninite melt evolution of the Cretaceous Kizildag (Turkey) ophiolite: model for multi-stage early arc-forearc magmatism in Tethyan subduction factories. Lithos 113, 68–87.
Droop, G.T.R., 1978. A general equation for estimating Fe3 + concentrations in ferromagnesian silicates and oxides from microprobe analysis, using stoichiometric criteria. Mineralogical Magazine 51, 431–435.
Duncan, R.A., Green, D.H., 1987. The genesis of refractory melts in the formation of oceanic crust. Contributions to Mineralogy and Petrology 96, 326–342.
Falloon, T.J., Crawford, A.J., 1991. The petrogenesis of high-calcium boninite lavas dredged from the northern Tonga ridge. Earth and Planetary Science Letters 102, 375–394.
Falloon, T.J., Danyushevsky, L.V., 2000. Melting of refractory mantle at 1·5, 2 and 2·5 GPa under anhydrous and H2O-undersaturated conditions: implications for the petrogenesis of high-Ca boninites and the influence of subduction components on mantle melting. Journal of Petrology 41, 257–283.
Falloon, T.J., Green, D.K., Crawford, A.J., 1987. Dredged igneous rocks from the northern termination of the Tofua magmatic arc. Tonga and adjacent Lau Basin. Australian Journal of Earth Sciences 34, 487–506.
Falloon, T.J., Malahoff, A., Zonenshain, L.P., Bogdanov, Y., 1992. Petrology and geochemistry of back-arc basin basalts from the Lau Basin spreading ridges at 15° 18° and19°S. Mineralogy and Petrology 47, 1–35.
Falloon, T.J., Danyushevsky, L.V., Crawford, A.J., Maas, R., Woodhead, J.D., Eggins, S.M., Bloomer, S.H., Wright, D.J., Zlobin, S.K., Stacey, A.R., 2007. Multiple mantle plume components involved in the petrogenesis of subduction related lavas from the northern termination of the Tonga Arc and northern Lau Basin: evidence from the geochemistry of arc and backarc submarine volcanics. Geochemistry, Geophysics, Geosystems 8, Q09003. doi:10.1029/2007GC001619.
Falloon, T.J., Danyushevsky, L.V., Crawford, A.J., Meffre, S., Woodhead, J.D., Bloomer, S.H., 2008. Boninites and adakites from the Northern termination of the Tonga Trench: implications for adakite petrogenesis. Journal of Petrology 49, 1–19.
Feng, Y.M., He, S.P., 1995. Research for geology and geochemistry of several ophiolites in the North Qilian Mountains, China. Geological Review 40, 252–264.
Flower, M.F.J., Levine, H., 1987. Petrogenesis of a tholeiite-boninite sequence from Ayio Mamas, Troodos ophiolite: evidence for splitting of a volcanic arc. Contributions to Mineralogy and Petrology 97, 509–524.
Hall, C.E., Gurnis, M., Sdrolias, M., Lavier, L.L., Müller, R.D., 2003. Catastrophic initiation of subduction following forced convergence across fracture zones. Earth and Planetary Science Letters 212, 15–30.
Hawkins, J.W., 1976. Petrology and geochemistry of basaltic rocks of the Lau Basin. Earth and Planetary Science Letters 28, 283–297.
Hawkins, J.W., Castillo, P.R., 1998. Early history of the Izu-Bonin-Mariana arc system: evidence from Belau and the Palau Trench. Island Arc 7, 559–578.
Hawkins, J.W., Bloomer, S.H., Evans, C.A., Melchior, J.T., 1984. Evolution of intra-oceanic arc-trench systerms. Tectonophysics 102, 175–205.
Hickey, R.L., Frey, F.A., 1981. Rare-earth element geochemistry of Mariana fore-arc volcanics: deep sea drilling project Site 458 and Hole 459B. In: Hussong, D.M., Uyeda, S., et al. (Eds.), Init. Rep. DSDP 60., 60, pp. 735–742.
Hickey, R.L., Frey, F.A., 1982. Geochemical characteristics of boninite series volcanics: implications for their source. Geochimica et Cosmochimica Acta 46, 2099–2115.

Hickey-Vargas, R., Reagan, M.K., 1987. Temporal variation of isotope and rare earth element abundances in volcanic rocks from Guam: implications for the evolution of the Mariana Arc. Contributions to Mineralogy and Petrology 97, 497–508.
Hou, Q.Y., Zh, Z.D., Zh, H.F., Zh, B.R., Ch, Y.L., 2006. Indian Ocean-MORB-type isotopic signature of Yushigou ophiolite in North Qilian Mountains and its implications. Science in China, Series D: Earth Sciences 49, 561–572.
Ishikawa, T., Nagaishi, K., Umino, S., 2002. Boninitic volcanism in the Oman ophiolite: implications for the thermal condition during transition from spreading ridge to arc. Geology 30 (10), 899–902.
Ishizuka, O., Kimura, J.-I., Li, Y.B., Stern, R.J., Reagan, M.K., Taylor, R.N., Ohara, Y., Bloomer, S.H., Ishii, T., Hargrove III, U.S., Haraguchi, S., 2006. Early stage in evolution of Izu-Bonin arc volcanism: new age, chemical, and isotopic constraints. Earth and Planetary Science Letters 250, 385–401.
Jaques, A.L., Chappell, B.W., 1980. Petrology and trace element geochemistry of the Papuan Ultramafic belt. Contributions to Mineralogy and Petrology 75, 55–70.
Jenner, G.A., 1981. Geochemistry of high-Mg andesites from Cape Vogel, Papua New Guinea. Chemical Geology 33, 307–332.
Kamenetsky, V.S., Crawford, A.J., Meffre, S., 2001. Factors controlling chemistry of magmatic spinel: an empirical study of associated olivine, Cr-spinel and melt inclusions from primitive rocks. Journal of Petrology 42, 655–671.
Kamenetsky, V.S., Sobolev, A.V., Eggins, S.M., Crawford, A.J., Arculus, R.J., 2002. Olivine-enriched melt inclusions in chromites from low-Ca boninites, Cape Vogel, Papua New Guinea: evidence for ultramafic primary magma, refractory mantle source and enriched components. Chemical Geology 183, 287–303.
Kelemen, P.B., Hanghøj, K., Greene, A.R., 2003. One view of the geochemistry of subduction-related magmatic arcs, with emphasis on primitive andesite and lower crust. In: Rudnick, R.L. (Ed.), Treatise on Geochemistry 3: The Crust. Elsevier, Amsterdam, pp. 593–659.
Kennish, M.J., Lutz, R.A., 1998. Morphology and distribution of lava flows on mid-ocean ridges: a review. Earth-Science Reviews 43, 63–90.
Kobayashi, K., 2004. Origin of the Palau. and Yap trench-arc systems. Geophysical Journal International 157, 1303–1315.
König, S., Münker, C., Schuth, S., Luguet, A., Hoffmann, J.E., Kuduon, J., 2010. Boninites as windows into trace element mobility in subduction zones. Geochimica et Cosmochimica Acta 74, 684–704.
Kurth-velz, M., Sassen, A., Suhr, G., Mezger, K., 1998. Precise ages and isotopic constraints for the Lewis Hills (Bay of Islands Ophiolite): Preservation of an arc-spreading ridge intersection. Geology 26, 1127–1130.
Kurth-velz, M., Sassen, A., Galer, S., 2004. Geochemical and isotopic heterogeneities along an island arc–spreading ridge intersections: evidence from the Lewis Hills, Bay of Islands ophiolite Newfoundland. Journal of Petrology 45, 635–668.
Liu, Y.J., Neubauer, F., Genser, J., Takasu, A., Ge, X.-H., Handler, R., 2006. 40Ar/39Ar ages of blueschist facies pelitic schists from Qingshuigou in the Northern Qilian Mountains, western China. Island Arc 15, 187–198.
MacLachlan, K., Dunning, G. Greg, 1998. U–Pb ages and tectonomagmatic relationships of early Ordovician low-Ti tholeiites, boninites and related plutonic rocks in central Newfoundland, Canada. Contributions to Mineralogy and Petrology 133, 235–258.
Macpherson, C.G., Hall, R., 2001. Tectonic setting of Eocene boninite magmatism in the Izu-Bonin-Mariana forearc. Earth and Planetary Science Letters 186, 215–230.
Meffre, S., Aitchison, J.C., Crawford, A.J., 1996. Geochemical evolution and tectonic significance of boninites and tholeiites from the Koh ophiolite, New Caledonia. Tectonics 15, 67–83.
Meijer, A., 1980. Primitive arc volcanism and boninite series: examples from western Pacific island arcs. In: Hayes, D.E. (Ed.), Tectonic and Geologic Evolution of Southwest Asian Seas and Islands: Am. Geophys. Union. Monogr., 23, pp. 269–282.
Meng, F.C., Zhang, J.X., Ker, C.M., Li, J.P., 2010. Constraints on the evolution of the North Qilian ocean basin: MOR-type and SSZ-type ophiolites from Dachadaban. Acta Petrologica Mineralogica 29 (5), 453–466.
Miyashiro, A., 1974. Volcanic rock series in island arcs and active continental margins. American Journal of Science 274, 321–355.
Monzier, M., Danyushevsky, L.V., Crawford, A.J., Bellon, H., Cotton, J., 1993. High-Mg andesites from the southern termination of the New Hebrides island arc (SW Pacific). Journal of Volcanology and Geothermal Research 57, 193–217.
Moore, J.G., 1970. Water content of basalt erupted on the ocean floor. Contributions to Mineralogy and Petrology 28, 272–279.
Moore, J.G., 1975. Mechanism of formation of pillow lava. American Scientist 63, 269–277.
Moore, J.G., Schilling, J.-G., 1973. Vesicles, water, and sulfur in Reykjanes Ridge basalts. Contributions to Mineralogy and Petrology 41, 105–118.
Moores, E.M., Robinson, P.T., Malpas, J., Xenophontos, C., 1984. A model for the origin of the Troodos massif, Cyprus, and other mideast ophiolites. Geology 12, 500–503.
Murton, B.J., Peate, D.W., Arculus, R.J., Pearce, J.A., Van der Laan, S.R., 1992. Trace-element geochemistry of volcanic rocks from Site 786: the Izu-Bonin forearc. In: Frey, P., Pearce, J.A., Stokking, L.B., et al. (Eds.), P Proc. ODP, Sci. Results, 125, pp. 211–235.
Mysen, B.O., Kushiro, I., 1977. Compositional variations of coexisting phases with degree of melting of peridotite in the upper mantle. American Mineralogist 62, 843–865.
Niedermeier, D., Bach, W., Beier, C., 2008. Evidence for boninite genesis in the Eastern Manus Basin. American Geophysical Union, Fall Meeting 2008, Abstract #V21A-2081.
Niu, Y.N., Collerson, K.D., 1999. Origin of enriched-type mid-ocean ridge basalt at ridges far from mantle plumes: the East Pacific Rise at 11°20′N. Journal of Geophysical Research 104, 7067–7087.
Niu, Y.N., O'Hara, M.J., 2008. Global correlations of ocean ridge basalt chemistry with axial depth: a new perspective. Journal of Petrology 49, 633–664.
Niu, Y.L., O'Hara, M.J., 2009. MORB mantle hosts the missing Eu (Sr, Nb, Ta and Ti) in the continental crust: new perspectives on crustal growth, crust–mantle differentiation and chemical structure of oceanic upper mantle. Lithos 112, 1–17.
Niu, Y.L., O'Hara, M.J., Pearce, J.A., 2003. Initiation of subduction zones as a consequence of lateral compositional buoyancy contrast within the lithosphere: A petrologic perspective. Journal of Petrology 44, 851–866.
Niu, Y.N., Regelous, M., Wendt, I.J., Batiza, R., O'Hara, M.J., 2002. Geochemistry of near-EPR seamounts: importance of source vs. process and the origin of enriched mantle component. Earth and Planetary Science Letters 199, 327–345.
Pagé, P., Bédard, J.H., Tremblay, A., 2009. Geochemical variations in a depleted fore-arc mantle: the Ordovician Thetford Mines ophiolite. Lithos 113, 21–47.
Pearce, J.A., 1983. Role of the sub-continental lithosphere in magma genesis at active continental margins. In: Hawkesworth, C.J., Norry, M.J. (Eds.), Continental Basalts and Mantle Xenoliths. Shiva, Nantwich, pp. 230–249.
Pearce, J.A., Peate, D.W., 1995. Tectonic implications of the composition of volcanic arc magmas. Annual Review of Earth and Planetary Sciences 23, 251–285.
Pearce, J.A., Robinson, P.T., 2010. The Troodos ophiolitic complex probably formed in a subduction initiation, slab edge setting. Gondwana Research 18, 60–81.
Pearce, J.A., Van der Laan, S.R., Arculus, R.J., Murton, B.J., Ishii, T., Peate, D.W., Parkinson, I.J., 1992. Boninite and Harzburgite from Leg125 (Bonin-Mariana Forearc): a case study of magma genesis during the initial stages of subduction. Proceedings of the Ocean Drilling Program - Scientific Results 125, 623–659.
Pearce, J.A., Baker, P.E., Harvey, P.K., Luff, I.W., 1995. Geochemical evidence for subduction fluxes, mantle melting and fractional crystallization beneath the South Sandwich Island Arc. Journal of Petrology 36, 1073–1109.
Peate, D.W., Pearce, J.A., Hawkesworth, C.J., Colley, H., Edwards, C.M.H., Hirso, K., 1997. Geochemical variations in Vanuatu arc lavas: the role of subducted material and a variable mantle wedge composition. Journal of Petrology 38, 1331–1358.
Pe-Piper, G., Tsikouras, B., Hatzipanagiotou, K., 2004. Evolution of boninites and island-arc tholeiites in the Pindos Ophiolite, Greece. Geological Magazine 141, 455–469.
Portnyagin, M.V., Danyushevsky, L.V., Kamenetsky, V.S., 1997. Coexistence of two distinct mantle sources during formation of ophiolites: a case study of primitive pillow lavas from the lowest part of the volcanic section of the Troodos Ophiolite, Cyprus. Contributions to Mineralogy and Petrology 128, 287–301.
Poustovetov, A.A., Roeder, P.L., 2001. The distribution of Cr between basaltic melt and chromian spinel as an oxygen geobarometer. The Canadian Mineralogist 39, 309–317.
Qian, Q., Zhang, Q., Sun, X.M., 2001. Tectonic setting and mantle source characteristics of Jiugequan basalts, North Qilian: constraints from trace elements and Nd-isotopes. Acta Geologica Sinica 17, 385–394.
Reagan, M.K., Meijer, A., 1984. Geology and geochemistry of early arc-volcanic rocks from Guam. Geological Society of America Bulletin 95, 701–713.
Rubin, K.H., Embley, R.W., Clague, D.A., Resing, J.A., Michael, P.J., Keller, N.S., Baker, E.T., 2009. Lavas from active boninite and very recent basalt eruptions at two submarine NE Lau Basin Sites. American Geophysical Union, Fall Meeting 2009, Abstract #V43I–05.
Salters, V.J.M., Stracke, A., 2004. Composition of the depleted mantle. Geochemistry, Geophysics, Geosystems 5, Q05004. doi:10.1029/2003GC000597.
Sameshima, T., Paris, J.P., Black, P.M., Heming, R.F., 1983. Clinoenstatite-bearing lava from Népoui, New Caledonia. American Mineralogist 68, 1076–1082.
Sharaskin, A.Y., 1981. Petrography and geochemistry of basement rocks from five Leg 60 Sites. In: Hussong, D.M., Uyeda, S., et al. (Eds.), Init. Rep. DSDP 60, pp. 647–656.
Shi, R.D., Yang, J.S., Wu, C.L., Wooden, J., 2004. The evidence of SHRIMP formed Late Sinina of Yushigou ophiolite in North Qilian Mountain. Acta Geologica Sinica 78, 649–657.
Sigurdsson, I.A., Kamenetsky, V.S., Crawford, A.J., Eggins, S.M., Zlobin, S.K., 2003. Primitive island arc and oceanic lavas from the Hunter Ridge-Hunter Fracture Zone: evidence from glass, olivine and spinel compositions. Mineralogy and Petrology 47, 149–169.
Smith, A.D., Yang, H.-Y., 2006. The neodymium isotopic and geochemical composition of serpentinites from ophiolitic assemblages in the Qilian fold belt, northwest China. Journal of Asian Earth Sciences 28, 119–132.
Sobolev, A.V., Danyushevsky, L.V., 1994. Petrology and geochemistry of boninites from the north termination of the Tonga Trench: constraints on the generation conditions of primary high-Ca boninite magmas. Journal of Petrology 35, 1183–1213.
Sobolev, A.V., Portnyagin, M.V., Dmitriev, L.V., Tsamerian, O.P., Danyushevsky, L.V., Kononkova, N.N., Shimizu, N., Robinson, P.T., 1993. Petrology of ultramafic lavas and associated rocks of the Troodos Massif, Cyprus. Petrology 1, 331–361.
Song, S.G., Su, L., 1998. Plastic rheology of the Yushigou mantle peridotite and implications for dynamics of Paleo-Plate movement in the North Qilian Mountains. Acta Geologica Sinica 72, 131–141.
Song, S.G., Zhang, L.F., Niu, Y.L., Song, B., Zhang, G.B., Wang, Q.J., 2004. Zircon U–Pb SHRIMP ages of eclogites from the North Qilian Mountains, NW China and their tectonic implication. Chinese Science Bulletin 49, 848–852.
Song, S.G., Zhang, L.F., Niu, Y., Su, L., Song, B., Liu, D.Y., 2006. Evolution from oceanic subduction to continental collision: a case study of the northern Tibetan Plateau inferred from geochemical and geochronological data. Journal of Petrology 47, 435–455.
Song, S.G., Zhang, L.F., Niu, Y., Wei, C.J., Liou, J.G., Shu, G.M., 2007. Eclogite and carpholite-bearing metasedimentary rocks in the North Qilian suture zone, NW China: implications for early Palaeozoic cold oceanic subduction and water transport into mantle. Journal of Metamorphic Geology 25, 547–563.
Song, S.G., Niu, Y.L., Zhang, L.F., Wei, C.J., Liou, J.G., Su, L., 2009a. Tectonic evolution of early Paleozoic HP metamorphic rocks in the North Qilian Mountains, NW China: new perspectives. Journal of Asian Earth Sciences 35, 354–366.

Song, S.G., Su, L., Niu, Y.L., Lai, Y., Zhang, L.F., 2009b. CH4 inclusions in orogenic harzburgite: evidence for reduced slab fluids and implication for redox melting in mantle wedge. Geochimica et Cosmochimica Acta 73, 1737–1754.
Song, S.G., Su, L., Li, X.H., Zhang, G.B., Niu, Y.L., Zhang, L.F., 2010. Tracing the 850-Ma continental flood basalts from a piece of subducted continental crust in the North Qaidam UHPM belt, NW China. Precambrian Research 183, 805–816.
Stacey, J.S., Kramers, J.D., 1975. Approximation of terrestrial lead isotope evolution by a two-stage model. Earth and Planetary Science Letters 26, 207–221.
Stern, R.J., 2004. Subduction initiation: spontaneous and induced. Earth and Planetary Science Letters 226, 275–292.
Stern, R.J., Bloomer, S.H., 1992. Subduction zone infancy: examples from the Eocene Izu-Bonin-Mariana and Jurassic California arcs. Geological Society of America Bulletin 104, 1621–1636.
Sugawara, T., 2000. Empirical relationships between temperature, pressure, and MgO content in olivine and pyroxene saturated liquid. Journal of Geophysical Research 105, 8457–8472.
Sun, S.-S., McDonough, W.F., 1989. Chemical and isotopic systematics of oceanic basalt: implications for mantle composition and processes. In: Saunders, A.D., Norry, M.J. (Eds.), Magmatism in the Ocean Basins: Geol. Soc. Spec. Publ., 42, pp. 313–345.
Tatsumi, Y., 1981. Melting experiments on a high-magnesian andesite. Earth and Planetary Science Letters 54, 357–365.
Tatsumi, Y., 1982. Origin of high-magnesian andesites in the Setouchi volcanic belt, southwest Japan II. Melting phase relations at high pressures. Earth and Planetary Science Letters 60, 305–317.
Tatsumi, Y., Sakuyama, M., Fukuyama, H., Kushiro, I., 1983. Generation of arc basalt magmas and thermal structure of the mantle wedge in subduction zones. Journal of Geophysical Research 88, 5815–5825.
Taylor, B., 1992. Rifting and the volcanic-tectonic evolution of the Izu-Bonin-Mariana arc. In: Taylor, B., Fujioka, K. (Eds.), Proc. ODP, Sci. Results, 126, pp. 627–651.
Taylor, B., Martinez, F., 2003. Back-arc basin basalt systematics. Earth and Planetary Science Letters 210, 481–497.
Taylor, R.N., Nesbitt, R.W., Vidal, P., Harmon, R.S., Auvray, B., Croudace, I.W., 1994. Mineralogy, chemistry, and genesis of the Boninite series volcanics, Chichijima, Bonin Islands, Japan. Journal of Petrology 35, 577–617.
Thy, P., Xenophontos, C., 1991. Crystallization orders and phase chemistry of glassy Lavas from the pillow sequences, Troodos ophiolite, Cyprus. Journal of Petrology 32, 403–428.
Tseng, C.Y., Yang, H.J., Yang, H.Y., Liu, D.Y., Tsai, C.L., Wu, H.Q., Zuo, G.C., 2007. The Dongcaohe ophiolite from the North Qilian Mountains: a fossil oceanic crust of the Paleo-Qilian ocean. Chinese Science Bulletin 52, 2390–2401.
Umino, S., 1986. Magma mixing in boninite sequence of Chichijima, Bonin Islands. Journal of Volcanology and Geothermal Research 29, 125–157.
Umino, S., Kushiro, I., 1989. Experimental studies on boninite petrogenesis. In: Crawford, A.J. (Ed.), Boninites and Related Rocks. Unwin Hyman, London, pp. 89–111.
Walker, D.A., Cameron, W.E., 1983. Boninite primary magmas: evidence from the Cape Vogel Peninsula, PNG. Contributions to Mineralogy and Petrology 83, 150–158.
Wang, C.Y., Zhang, Q., Qian, Q., 2005. Geochemistry of the Early Paleozoic Baiyin volcanic rocks (NW China): implications for the tectonic evolution of the North Qilian Orogenic Belt. Journal of Geology 113, 83–94.
Wendt, J.I., Regelous, M., Collersonm, K.D., Ewart, A., 1997. Evidence for a contribution from two mantle plumes to island-arc lavas from northern Tonga. Geology 25, 611–614.
Wood, C.P., 1980. Boninite at a continental margin. Nature 288, 692–694.
Workman, R.K., Hart, S.R., 2005. Major and trace element composition of the depleted MORB mantle (DMM). Earth and Planetary Science Letters 231, 53–72.
Wu, H.Q., Feng, Y.M., Song, S.G., 1993. Metamorphism and deformation of blueschist belts and their tectonic implications, North Qilian Mountains, China. Journal of Metamorphic Geology 11, 523–536.
Wu, C.L., Xu, X.Y., Gao, Q.M., Li, X.M., Lei, M., Gao, Y.H., Frost, R.B., Wooden, J.L., 2010. Early Palaezoic grranitoid magmatism and tectonic evolution in North Qilian. Acta Petrolei Sinica 26, 1027–1044.
Xia, X.H., Song, S.G., 2010. Forming age and tectono-petrogenesis of the Jiugequan ophiolite in the North Qilian Mountain, NW China. Chinese Science Bulletin 55, 1899–1907.
Xia, L.Q., Xia, Z.C., Xu, X.Y., 2003. Magmagenesis in the Ordovician backarc basins of the northern Qilian Mountains, China. Geological Society of America Bulletin 115, 1510–1522.
Xiao, X.C., Chen, G., Zhu, Z.Z., 1978. A preliminary study on the tectonics of ancient ophiolites in the Qilian Mountain, Northwest China. Acta Geologica Sinica 52, 281–295.
Yuan, C., Sun, M., Li, J.L., Hou, Q.L., Zhou, M.F., 2002. Tectonic background of the Kuda ophiolite, western Kunlun: new constraints from boninite series rocks. Geochimica 31, 43–46.
Zhang, J.X., Xu, Z.Q., Chen, W., Xu, H.F., 1997. A tentative discussion on the ages of the subduction-accretionary complex/volcanic arcs in the middle sector of North Qilian Mountain. Acta Petrologica Mineralogica 16 (2), 112–119.
Zhang, Q., Chen, Y., Zhou, D.J., Qian, Q., Jia, X.Q., Han, S., 1998. Geochemical characteristics and genesis of Dachadaban ophiolite in North Qilian area. Science in China, Series D: Earth Sciences 41, 277–281.
Zhang, J.X., Meng, F.C., Wan, Y.S., 2007. A cold early Palaeozoic subduction zone in the North Qilian Mountains, NW China: petrological and U–Pb geochronological constraints. Journal of Metamorphic Geology 25, 285–304.